Title

Cyclic Fatigue of Ceramics: A Fracture Mechanics Approach to Subcritical Crack Growth and Life Prediction

Authors

Ritchie, R.O.
Dauskardt, R.H.

Publication Date

1991-03-01

LBL-30449
Preprint

Center for Advanced Materials

CAM

Submitted to the Journal of the Ceramic Society of Japan

Cyclic Fatigue of Ceramics: A Fracture Mechanics Approach to Subcritical Crack Growth and Life Prediction

R.O. Ritchie and R.H. Dauskardt

March 1991

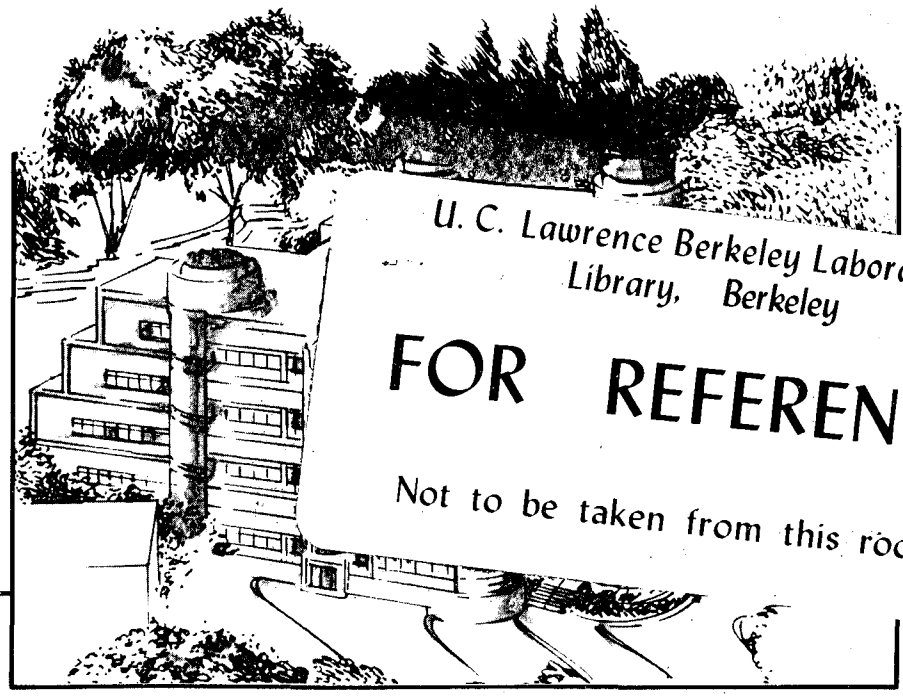

Materials and Chemical Sciences Division

Lawrence Berkeley Laboratory • University of California

ONE CYCLOTRON ROAD, BERKELEY, CA 94720 • (415) 486-4755

Prepared for the U.S. Department of Energy under Contract DE-AC03-76SF00098

DISCLAIMER

LBL-30449

CYCLIC FATIGUE OF CERAMICS: A FRACTURE MECHANICS APPROACH TO SUBCRITICAL CRACK GROWTH AND LIFE PREDICTION

R. O. Ritchie and R. H. Dauskardt

Center for Advanced Materials, Materials Sciences Division
Lawrence Berkeley Laboratory
and
Department of Materials Science and Mineral Engineering
University of California, Berkeley, CA 94720

March 1991

to be published in

Journal of the Ceramic Society of Japan
volume 99, 1991

This work was supported by the Director, Office of Energy Research, Office of Basic Energy Sciences, Materials Sciences Division of the U.S. Department of Energy under Contract No. DE-AC03-76SF00098 (for work on monolithic ceramics), and by the U.S. Office of Naval Research under Grant No. N00014-89-J-1094 (for work on composites).

Cyclic Fatigue of Ceramics: A Fracture Mechanics Approach to Subcritical Crack Growth and Life Prediction

R. O. RITCHIE and R. H. DAUSKARDT

Center for Advanced Materials, Materials Sciences Division, Lawrence Berkeley Laboratory, and Department of Materials Science and Mineral Engineering, University of California, Berkeley, CA 94720, U.S.A.

Cyclic fatigue, and specifically fatigue-crack propagation, in ceramic materials is reviewed both for monolithic and composites systems. In particular, stress/life (S/N) and crack-propagation data are presented for a range of ceramics, including zirconia, alumina, silicon nitride, SiC-whisker-reinforced alumina and a pyrolytic-carbon/graphite laminate. S/N data derived from unnotched specimens often indicate markedly lower lives under tension-compression compared to tension-tension loading; similar to metals, 10^8-cycle "fatigue limits" generally approach ~50% of the tensile strength. Crack-growth results, based on studies on "long" (>3 mm) cracks, show fatigue-crack propagation rates to be markedly power-law dependent on the applied stress-intensity range, ΔK, with a threshold, ΔK_{TH}, of the order of ~50% of K_c. Conversely, for "small" (<250 μm) surface cracks, fatigue-crack growth is seen to occur at ΔK levels some 2 to 3 times smaller than ΔK_{TH}, and to show a negative dependency on applied stress intensity. At ambient temperatures, lifetimes are shortened and crack-growth rates are significantly accelerated by cyclic, compared to quasi-static, loading, although limited results suggest the reverse to be true at very high temperatures in the creep regime. Such results are discussed in terms of the primary crack-tip shielding (toughening) mechanisms and potential mechanisms of cyclic crack advance. Finally, implications are discussed of long and small crack cyclic fatigue data to life prediction and safety-critical design with ceramic components.

Key-words: Cyclic fatigue, crack growth, small cracks, fatigue threshold, ceramics, ceramic-matrix composites, Mg-PSZ, alumina, silicon nitride, SiC-reinforced alumina, pyrolytic-carbon/graphite laminate, damage-tolerant design, life prediction

1. Introduction

The importance of mechanical degradation under cyclic fatigue loading in the design of metallic structures and components is characterized by either a classical stress/life (S/N) approach or using fracture mechanics concepts which incorporate the subcritical growth behavior of both "long" and "small" cracks (Fig. 1). Over the past few years, several studies have provided persuasive evidence of a similar susceptibility of ceramic and ceramic-matrix composite materials to cyclic fatigue. In fact, extensive data have now been reported indicating reduced lifetimes during S/N testing under cyclic, compared to sustained (quasi-static), loads, and accelerated cyclic crack-propagation rates at stress intensities less than required for environmentally-enhanced

crack growth (static fatigue) during fracture-mechanics testing; results exist for zirconia,[1)-11)] graphite,[12)] alumina,[6),13)-24)] silicon nitride[16),25)-29)] and silica glass[30)] ceramics and LAS/SiC_f,[31)] Al_2O_3/SiC,[32)-34)] and laminated graphite/pyrolytic carbon[12)] composites.

While the precise micro-mechanisms for such cyclic fatigue are still unclear, behavioral characteristics are in general *qualitatively* similar to those in metallic materials. For example, typical ambient-temperature stress/life data for alumina, TZP, silicon nitride and silicon carbide, taken from the four-point bend (zero-tension) data of Kawakubo *et al.*,[6)], are shown in Fig. 2. It is clear that for lives in excess of $\sim 10^3$ cycles, the time to failure under cyclic loads is less than that under quasi-static loads at the same maximum stress, and further, with the exception of SiC, the cyclic fatigue life is less than that predicted using the static data by integrating over the fatigue cycle. However, the inverse slope, n, of these curves is far higher than that found in metals; values range from 11 in TZP to 132 in SiC.

Alternatively, typical crack-propagation data (long crack), taken from the authors' own ambient-temperature studies [1),4),12),33)] on compact-tension specimens, are shown in Fig. 3; these results illustrate the dependency of cyclic fatigue-crack growth rates, da/dN, on the applied (far-field) stress-intensity range ($\Delta K = K_{max} - K_{min}$), for three zirconia ceramics, graphite, a pyrolytic-carbon-coated graphite laminate and a SiC-whisker-reinforced alumina (Al_2O_3-SiC_w) composite, and are compared with similar data for steel and aluminum high-strength metallic alloys.[35),36)] Similar to metals, the ceramic fatigue data follow a Paris power-law relationship[37)] of the form:

$$da/dN = C(\Delta K)^m , \qquad (1)$$

where C and m are scaling constants; the exponent, m, however, varies between 12 to over 40, which is far higher than the typical values of between 2 and 4 generally found for metals in this regime.

In addition to such crack-propagation data for "long" cracks (typically longer than $\sim$3 mm), more recent results[7)-10),16),26),29)] on cracks which are physically small (typically smaller than $\sim$500 μm) or approach the dimensions of the microstructure or local crack-tip inelasticity, have shown radically different growth behavior. Again, similar to behavior widely reported for metals,[38)] crack-propagation rates for such "small" surface cracks have been observed to far exceed those of "long" cracks at equivalent applied stress-intensity levels, and more importantly to occur at stress

intensities *less than* the fatigue threshold, ΔK_{TH}, below which (long) cracks are presumed to be dormant.[7)-9)]

Accordingly, the objective of this review is to survey current understanding of the cyclic fatigue behavior of monolithic and reinforced ceramics, with respect to stress/life and crack-propagation data under both constant and variable-amplitude loading. Long and microstructurally-small crack-growth behavior will be reviewed and possible micro-mechanisms advanced. Finally, the implications for fatigue life prediction and design criteria for ceramic components are discussed.

2. Testing Methods

2.1 Stress/life testing

In general, stress/life (S/N) cyclic fatigue tests on ceramic materials have been performed in similar fashion to the standard techniques used for metallic materials, although much greater care has been required in the design of the loading grips. Techniques include zero-tension and tension-tension testing in cantilever bend and three- and four-point bending,[6),9),25)] tension-compression testing in rotary bending,[14),18)] and uniaxial push-pull, and tension-torsion testing.[27)] Typical stress/life results are shown in Fig. 2.

2.2 Constant-amplitude crack-propagation testing

Cyclic fatigue-crack propagation studies on through-thickness long cracks have been conducted on a variety of pre-cracked fracture mechanics samples; results have been reported for single-edge-notched specimens in three- and four-point bending, single- and double-anvil configured specimens in bending, tapered double-cantilever beam specimens and compact-tension C(T) specimens. The system used by the current authors, illustrated in Fig. 4a, utilizes ~1 to 6 mm thick C(T) specimens which are cycled at various positive load ratios (R = ratio of minimum to maximum loads) at frequencies up to 50 Hz.[1),4)] Following crack initiation from a wedge-shaped starter notch,[1)] crack-growth rates are determined over the range $\sim 10^{-12}$ to 10^{-4} m/cycle using computer-controlled K decreasing and K increasing conditions; applied loads are varied such that the instantaneous values of the crack length, a, and stress-intensity range, ΔK, vary according to the equation:

$$\Delta K = \Delta K_o \exp[C^*(a - a_o)] , \quad (2)$$

where a_o and ΔK_o are the initial values of a and ΔK, and C^* is the normalized K gradient [(1/K)(dK/da)] set typically to ± 0.08 mm^{-1}. Linear elastic stress-intensity solutions for the various specimen geometries are given in standard handbooks.[39)]

As an alternative to optical crack-length measurements, electrical-resistance techniques, using ~0.1 μm NiCr films evaporated onto the specimen surface, can be employed to continuously monitor *in situ* the crack length to a resolution of within ± 5 μm.[1),4)] In addition, unloading compliance measurements using back-face strain gauges have been utilized[4)] to assess the extent of fatigue crack closure caused by premature contact of the crack surfaces during the loading cycle. This is achieved by defining a far-field stress intensity, K_{cl}, at first contact of the crack surfaces during the unloading cycle, i.e., at the highest load where the elastic unloading compliance deviates from linearity.[36)] In metal fatigue, the value of the closure stress intensity is often used to compute an effective (near-tip) crack-driving force given by the difference of the maximum stress intensity and K_{cl}, i.e., $\Delta K_{eff} = K_{max} - K_{cl}$ (where $K_{cl} > K_{min}$).

Corresponding fatigue-crack propagation data for small (<250 μm) surface cracks has generally been determined through replication or optical examination of the top surface of cantilever-beam specimens loaded in tension-compression (Fig. 4b); depending upon the ease of crack initiation, such specimens are either unnotched or contain stress concentrators such as micro-hardness indents or a notch. Ideally tests are interrupted after ~100 cycles to ascertain damage accumulation during initial loading and then subsequently at 10^2 to 10^3 cycle intervals until failure.[8)] Small-crack lengths can be readily quantified, with a resolution better than ± 0.5 μm by digitizing optical micrographs of the specimen surface using an image analyzer, in order to compute growth rates between ~10^{-12} to 10^{-6} m/cycle. Stress-intensity factors for such surface cracks can be obtained from linear elastic solutions [40)] for three-dimensional semi-elliptical surface cracks in bending (and/or tension) (Fig. 2b) in terms of crack depth a, crack length c, elliptical parametric angle ϕ, shape factor Q, specimen width t, specimen thickness B, and remote (outer surface) bending stress, σ_b:

$$K = H_c \sigma_b (\pi a/Q)^{1/2} F(a/c, a/t, c/B, \phi), \quad (3)$$

where H_c is the bending multiplier and F is a boundary correction factor (Fig. 4b).

2.3 Variable-amplitude crack-propagation testing

Limited results have also been reported by the authors for cyclic fatigue-crack propagation behavior in ceramic materials during variable-amplitude loading sequences.[5),33)] Such tests have been performed on long cracks, specifically in transformation-toughened Mg-PSZ and a SiC-whisker-reinforced alumina, by applying various load excursions during steady-state fatigue-crack growth, and monitoring the transient crack-growth response as a function of crack extension until steady-state growth is re-established. The principal loading spectra that have been used include single tensile overloads and block-loading sequences (both low-high and high-low), comprising selected constant stress-intensity ranges. In addition, growth rates have been examined under constant K_{max}/variable-R conditions, where the maximum stress intensity is held constant as K_{min} is increased; such loading spectra have been used in metal fatigue studies to minimize the influence of crack closure on growth-rate behavior.[41)]

3. Stress-Life Behavior

As noted above, cyclic stress/life (S/N) data for most ceramic materials at ambient temperatures show lifetimes to be less than that to cause failure at the same maximum stress under quasi-static loads, and to be less than that predicted from the static stress/life data assuming only time-dependent (and not cycle-dependent) processes.[6),25)] As in metals, the fatigue strength decreases with number of cycles, although the dependence of life on applied stress, i.e., the inverse slope, n, of the S/N curve is far higher; typical values are listed in Table 1. In addition, S/N curves appear to be much more sensitive to the load ratio than with metallic materials.[10)]

S/N curves on *unnotched* cantilever-beam samples of mid-toughness (MS grade) and overaged (pre-transformed) Mg-PSZ, under both zero-tension (R = 0) and tension-compression (R = -1) loading, are shown in Fig. 5;[7),8)] corresponding data from Swain *et al.*[2)] for MS-grade Mg-PSZ, tested in four-point bend (R = 0) and rotating bend (R = -1), are included for comparison. It is apparent that, similar to behavior in steels, the MS-grade material shows evidence of a "fatigue limit" of roughly 50% of the single-cycle tensile (or bending) strength, at 10^8 cycles (R = -1). However, not all ceramics have such a distinct knee in the S/N curve above 10^6 cycles; sintered alumina, for example, can fail at lives in excess of 10^8 cycles, with a 10^8-cycle endurance strength some 25 to 40% of the single-cycle strength.[18)]

Similar to results reported for Si_3N_4,[25),27)] the Mg-PSZ data in Fig. 5 also indicate that cycling in tension-compression is significantly more damaging than in tension. This is apparent from optical examination[8)] of specimen surfaces in MS-grade material at both R-ratios, where quantitative analysis of the crack-size distributions reveals an increased distribution of larger microcracks at R = -1 (Fig. 6). Microcracks appear in regions of surface uplift from transformation and their alignment is primarily orthogonal to the stress axis, although some cracks form at angles of ~45° to the stress axis at R = -1.

This effect, however, is not general to ceramic fatigue. Unlike results on smooth samples,[7),8),26)] S/N data derived from results on *micro-indented* cantilever-bend specimens, of a SiC-whisker-reinforced alumina,[33)] show no such difference between tension-compression and tension-tension cycling (Table 2). This may be because fully reversed cyclic loading has a greater effect on *initiating* fatigue damage in the form of microcracks, which in unnotched samples can account for a significant proportion of the life. In fact, it is known that where defects pre-exist (as micro-indents), lifetimes in tension and tension-compression are comparable as *crack-growth rates* are similar (Fig. 7).[33)]

4. Fatigue-Crack Propagation Behavior

4.1 Long-crack behavior

The variation in cyclic fatigue-crack propagation rates with the applied stress-intensity range, shown in Fig. 1 for long cracks in an range of ceramic materials, illustrates the extremely high dependency of da/dN on ΔK. Similar results are apparent for several transformation-toughened (sub-eutectoid aged) and pre-transformed (overaged) microstructures in Mg-PSZ[4)] (Fig. 8a), SiC-whisker-reinforced alumina (Fig. 9),[33)] silicon nitride,[29)] silica glass,[30)] and a pyrolytic-carbon coated graphite laminate[12)] (Fig. 10). As noted above, these data in general conform to a power-law relationship (Eq. 1) over the mid-range of growth rates, with very high exponents (i.e., the slope m of the da/dN vs. ΔK curve). Values of m, listed for several ceramics in Table 2, can vary between ~10 and over 100; the constant C, on the other hand, appears to scale inversely with the fracture toughness K_c. Fatigue threshold ΔK_{TH} values may be defined at a maximum growth rate of $\sim 10^{-10}$ m/cycle since the da/dN(ΔK) curves do not always show a sigmoidal shape; these values are typically of the order of 50% of K_c.

In view of past skepticism over the fatigue of ceramics, experiments have been performed to demonstrate unequivocally that crack growth in these instances is cyclically induced and not simply a consequence of stress-corrosion cracking (static fatigue).[4),12)] To achieve this, crack extension has been monitored at constant K_{max} with varying K_{min}, as shown for a pyrolytic-carbon/graphite laminate in Fig. 11. It is apparent that, whereas crack extension proceeds readily under cyclic loading conditions (region a), upon removal of the cyclic component by holding at the same K_{max} (region b), crack-growth rates are markedly reduced. Aside from establishing that the crack-growth behavior is a true cyclic fatigue phenomenon, this result illustrates that subcritical crack-growth rates due to cyclic fatigue are far in excess of those due to static fatigue at the same K_{max}.[1)]

In certain experiments, crack closure has been observed during fatigue-crack growth in ceramics; results are shown in Fig. 12 for four microstructures in Mg-PSZ with increasing degrees of transformation toughening.[4)] In metals, such closure primarily results from premature contact between the crack surfaces by fracture-surface asperities, and can have a potent influence in *locally* affecting the "crack-driving force".[42),43)] The degree of closure in ceramics, however, appears to be smaller, and in materials like Mg-PSZ is dwarfed by other mechanisms of crack-tip shielding such as transformation toughening.[4)] In fact, resistance to cyclic fatigue-crack extension in Mg-PSZ is observed to increase directly with the degree of crack-tip shielding resulting from increased transformation toughening (Fig. 8a). Such crack-growth data can therefore be normalized to a single curve (Fig. 8b) by characterizing in terms of the near-tip stress-intensity range, ΔK_{tip}, which allows for the extent of shielding, as outlined below.[4)]

In Mg-PSZ, the tetragonal phase, which typically consists of approximately 40 vol% of lens-shaped precipitates of maximum size ~300 nm, can undergo a stress-induced martensitic transformation to a monoclinic phase in the high stress field near the crack tip. The resultant dilatant transformation zone in the wake of the crack exerts compressive tractions on the crack surfaces which shield the crack tip from the applied (far-field) stresses.[44)-46)] The crack-tip stress intensity, K_{tip}, is therefore reduced from the applied (far-field) K by a shielding stress intensity, K_s, which is dependent upon the volume fraction, f, of the transforming phase within the zone, the width of the zone w, and the dilatational component of the transformation strain ϵ^T, Young's modulus E, Poisson's ratio ν, and a constant A dependent on the frontal zone shape:[47),48)]

$$K_{tip} = K - K_s \ , \qquad (4)$$

$$K_s = A(E/1 - \nu^2)\epsilon^T f w^{1/2} \quad . \tag{5}$$

Under cyclic loading, shielding from transformation far exceeds that due to crack closure; accordingly, the *local* near-tip stress-intensity range can be expressed by:[4)]

$$\Delta K_{tip} = K_{max} - K_s \quad , \tag{6}$$

By computing K_s using the integrated form of Eq. 5 and Raman spectroscopy measurements of the transformation-zone size,[4),5),49),50)], growth rates can be characterized in terms of ΔK_{tip}, thereby accounting for the differing fatigue resistance of the four microstructures (Fig. 8b). An equivalent result can be achieved by normalizing the crack-growth data in terms of $\Delta K/K_c$.[4)]

Fractographically, little discernible difference is generally apparent between monotonic and fatigue fracture surfaces in ceramics; this is in marked contrast to metals where clear distinction is generally observed between striation growth under cyclic loads and microvoid coalescence or cleavage, for instance, under quasi-static loads.[35)] Fatigue and fracture surfaces in silicon carbide, graphite, pyrolytic carbon, and Mg-PSZ are essentially identical;[4),51)] in Mg-PSZ, for example, surfaces are primarily transgranular with crack paths showing evidence of crack deflection, branching, and uncracked-ligament bridging behind the crack tip. In certain ceramics, however, the fractography of the resulting cyclic and monotonic fracture surfaces do show some distinction. An example of this is Al_2O_3-SiC_w.[33)] Fatigue fracture surfaces appear to be more textured and rougher with a higher degree of SiC whisker pull out than monotonic fracture surfaces. At higher magnification, crack paths formed under monotonic loading can be seen to be predominantly transgranular, with a high incidence of cleavage steps (indicated by arrows on the micrograph) and a flatter appearance (Fig. 13a,b). The increased roughness of the fatigue surfaces, conversely, appears to be associated with an increasing degree of intergranular fracture (Fig. 13c,d).

4.2 Small-crack behavior

The question of small cracks is undoubtedly of special importance to ceramics simply because the majority of ceramic components in service will not be able to tolerate the presence of physically long cracks. In metal fatigue, it is known that where crack sizes approach the dimensions of the microstructure or the extent of local crack-tip plasticity, or where cracks are simply physically small (typically $\lesssim$250 μm), the

similitude of crack-tip field characterization can break down (see, for example ref. 38). Specifically, small-crack growth rates are often far in excess of those of corresponding long cracks at the same applied ΔK levels; moreover, small-crack growth can occur at stress intensities well below the (long-crack) threshold ΔK_{TH}. Although such apparently anomalous behavior can be attributed to a number of factors,[38] the primary reason is that the extent of crack-tip shielding (in metals, principally from crack-closure phenomena) is generally diminished in small flaws by virtue of their limited wake.[36] In fact, a more precise definition of a small crack is one whose length is small relative to the size of the shielding zone. Since crack-tip shielding, from phase transformation, microcracking, crack bridging etc., plays a pivotal role in the toughening of many monolithic and composite ceramics, it is to be expected that such small-crack effects may also be prevalent in ceramic fatigue behavior.

Results on small fatigue cracks in ceramics, however, are very limited.[7)-10),29),33)] Typical crack-growth data for Mg-PSZ, monitored from unnotched cantilever-beam S/N samples and characterized in terms of the applied K_{max}, are compared to corresponding long-cracks data in Fig. 14a.[7),8)] In sharp contrast to long-crack results, the small cracks grow at progressively decreasing growth rates with increase in size, until finally linking together as the density of cracks across the specimen surface increases; the specimen then fails. Small-crack propagation rates display a negative, non-unique dependency on stress intensity and occur at applied stress-intensity levels well below ΔK_{TH} (specifically at K_{max} levels of 1.6 MPa$\sqrt{m}$, *a factor of seven less than* K_c). Moreover, growth rates are clearly not a unique function of K_{max} and appear to be sensitive to the level of applied stress.

Similar behavior has been reported for ceramic composites.[33)] The crack lengths of selected microcracks at similar maximum applied stress levels, emanating from micro-indents in cantilever-beam samples of SiC-whisker-reinforced alumina, are compared as a function of number of cycles at R = 0.05 and -1 in Fig. 15. As in monolithic ceramics, the small cracks grow at progressively decreasing growth rates, i.e., when plotted as propagation rates as a function of the applied K_{max} (Fig. 9), the crack-growth rate data display a characteristic negative dependency on applied stress intensity.

Such sub-threshold small-crack growth behavior can be explained by analogy to small-crack behavior in metals (e.g., refs. 36,38). Although the nominal (far-field) stress intensity K increases with increase in crack size, the shielding stress intensity K_s is also enhanced as a shielding zone is developed in the crack wake. The near-tip stress intensity (Eq. 6) and hence the crack-growth behavior is thus a result of the mutual

competition between these two factors; initially K_{tip} is diminished with crack extension until a steady-state shielding zone is established, whereupon behavior approaches that of a long crack. In Mg-PSZ, the primary shielding is due to phase transformation, whereas in the Al_2O_3/SiC_w composite, it is presumed to result from crack bridging by unbroken whiskers in the crack wake,[33] and from the residual stress field surrounding the micro-indent.

With a detailed knowledge and quantitative modelling of the salient shielding mechanisms, it is possible to normalize long and small crack data by characterizing in terms of the near-tip or net stress intensity, K_{tip}, i.e., after subtracting out the stress intensity due to shielding. Computations of K_s and hence K_{tip} have been achieved for small fatigue cracks in a SiC-fiber-reinforced LAS glass-ceramic, where the predominant shielding resulted from fiber bridging,[31] and in Al_2O_3, Si_3N_4 and 3Y-TZP where the effect of the residual stress field associated with the crack-initiating micro-indents was taken into account.[10),16),26] This is illustrated in Fig. 16 where small and long crack data in 3Y-TZP are normalized by defining K_{tip} in terms of a superposition of the applied and residual stress fields.[10] In addition, long-crack data in Mg-PSZ has been characterized in terms of K_{tip} in Fig. 14b after correcting for transformation shielding;[8] it is apparent that the da/dN ($K_{tip,max}$) curve corresponds closely to that associated with the initial growth of the small cracks. However, whether such analytical procedures to normalize small and long crack data are practical on a regular engineering basis for all ceramic materials in service is clearly questionable.

4.3 Variable-amplitude loading

In addition to the cyclic fatigue of ceramics under constant-amplitude loading data described above, limited studies have been performed to examine crack-propagation behavior under variable-amplitude loading. These studies have been focused on the transient crack-growth response to single tensile overload, block loading and constant-K_{max}/variable-R (increasing K_{min}) sequences during steady-state fatigue-crack growth, specifically in MS-grade Mg-PSZ[5] and a SiC-whisker-reinforced Al_2O_3 composite.[33]

Behavior in Mg-PSZ, shown for MS- and TS-grades in Fig. 17,[5] is similar to that widely reported in metals (e.g., ref. 52). In Fig. 17a, a high-low block overload, from a ΔK of 5.48 to 5.30 MPa$\sqrt{m}$, is first applied to an MS-grade sample; on reducing the cyclic loads, an immediate transient retardation is seen followed by a gradual increase in growth rates until the (new) steady-state velocity is achieved.

Similarly, by subsequently increasing the cyclic loads so that $\Delta K = 5.60$ MPa$\sqrt{m}$ (low-high block overload), growth rates show a transient acceleration before decaying to the steady-state velocity. The increment of crack growth over which the transient behavior occurs is ~700 μm, approximately five times the measured[5),49)] transformed-zone width of ~150 μm. This is consistent with zone-shielding calculations which compute the maximum steady-state shielding to be achieved after crack extensions of approximately five times the zone width.[47),48)] In fact, relatively accurate predictions of the post load-change transient crack-growth behavior have been obtained (dotted line in Fig. 17a) by computing the extent of crack-tip shielding in the changing transformation zone following the load changes.[5)] The changing size of the crack-tip transformation zone can be readily mapped using spatially-resolved Raman spectroscopy techniques.[49)] For example, zone sizes for the block-loading sequence on TS-grade material shown in Fig. 17b are illustrated in Fig. 18.[5)] In general, the significant variation in growth rates with small changes in ΔK is consistent with the steep slope of the da/dN-ΔK curves (Eq. 1) found in ceramics.

In contrast, variable-amplitude loading in the Al_2O_3-SiC_w composite is quite different (Fig. 19).[33)] Over the first ~1.2 mm of crack advance, the crack-growth rate remains approximately constant at a baseline ΔK of 3.6 MPa$\sqrt{m}$. On reducing the cyclic loads so that $\Delta K = 3.2$ MPa$\sqrt{m}$ (high-low block overload), crack-growth rates decrease by a ~1.5 orders of magnitude; by subsequently increasing the cyclic loads to a ΔK of 3.6 MPa$\sqrt{m}$ (low-high block overload), growth rates increase to previous baseline levels. Unlike Mg-PSZ where marked transient growth-rate effects result from transformation-zone shielding, the Al_2O_3-SiC_w composite, which is presumed to undergo crack bridging by intact whiskers spanning the crack, does not show such transient behavior; the scatter in growth rates, however, is large.

The precise role of variable-amplitude loading on cyclic crack growth in the various ceramic systems is still uncertain. It is known that in metals and phase-transforming ceramics, an overload cycle creates an enlarged crack-tip plastic or transformation zone which then promotes crack-growth retardation by reducing the near-tip stress intensity by residual compressive stress and resulting crack-closure effects in metals or by transformation shielding in the ceramics.[5),52)] However, in the non-transforming ceramics, such as Al_2O_3/SiC_w which may rely on shielding by crack bridging, the overload cycle may enhance shielding by increasing the extent of the bridging zone in the crack wake, or conversely diminish shielding by causing the failure of more bridges. Resolution of this effect must await more detailed bridging

calculations and experimental measurements of the bridging-zone sizes following various loading sequences.

4.4 High temperature fatigue

Despite the anticipated high-temperature use of ceramics in service applications, studies on the cyclic fatigue of monolithic and composite ceramics at elevated temperatures are extremely limited.[2),11),22),32),34),53)] However, studies on the S/N behavior of MS- and TS-grade Mg-PSZ using 100 Hz rotational flexture (R = -1) tests at moderately high temperatures up to 400°C in air clearly show a progressive decrease in fatigue resistance with increase in temperature, concurrent with a general increase in the inverse slope, e.g., the exponent, n, varies from 34 at 20°C to 116 at 200°C in TS-grade material.[2)] Resistance to cyclic fatigue-crack propagation rates is similarly diminished in Mg-PSZ at these temperatures; in TS-grade material, ΔK_{TH} thresholds have been reported to drop from 3.5 MPa$\sqrt{m}$ at 20°C to 3.0 MPa$\sqrt{m}$ at 650°C, with the exponent, m, increasing from 25 to 70 over the same temperature range.[11)]

At high homologous temperatures in the creep regime, however, cyclic fatigue mechanisms in ceramics do not appear to be as damaging as static fatigue or creep mechanisms. For example, S/N uniaxial tensile fatigue studies on alumina at 1200°C reveal the lives of samples loaded in cyclic fatigue (R = 0.1) in general to exceed those loaded quasi-statically at the same maximum stress (Fig. 20).[22)] Cyclic fatigue lifetimes were found to be dependent upon the frequency and cyclic waveform, specifically to the duration of the application of the maximum stress. In fact, assuming only time- (and not cycle-) dependent processes, cyclic lifetimes predicted from the static fatigue data were in general less than measured lifetimes, in sharp contrast to behavior at ambient temperatures (Fig. 2a). Similar results have been reported for hot pressed Si_3N_4 at 1200°C.[53)] Corroborating evidence from crack-propagation studies in alumina at 1050°C and SiC-whisker-reinforced alumina at 1400°C (frequency = 2 Hz, R ~ 0.1) show the cyclic crack-growth rates to be less than those measured under static loading at the same applied maximum stress intensity (Fig. 21).[32)] In these cases, the improved cyclic fatigue resistance has been attributed, at least in part, to the bridging of crack surfaces by the glassy phase, present in grain boundaries or formed *in situ* by the oxidation of the SiC whiskers.

5. Mechanisms of Ceramic Fatigue

In metals, mechanisms of cyclic fatigue have been based primarily on crack-tip dislocation activity leading to crack advance via such processes as alternating blunting and resharpening of the crack tip.[54] Accordingly, the refuted existence of a true fatigue effect in ceramics has been based in the past on the very limited crack-tip plasticity in these materials. However, it is now apparent that other inelastic deformation mechanisms may prevail; these mechanisms include microcracking and transformation "plasticity" in monolithic materials, the frictional sliding or controlled debonding between the reinforcement phase and ceramic matrix in brittle fiber or whisker reinforced composites, and the plastic deformation of a metallic or intermetallic phase itself in ductile-particle toughened composites. In fact, these factors are the prime reason for marked resistance-curve (R-curve) fracture-toughness properties of ceramic composites,[55] as such crack-tip shielding mechanisms develop progressively (until steady state) with increasing initial crack extension. Such deformation processes, like dislocation activity in metals, can similarly contribute to fatigue damage due to their nonlinear irreversible nature, although the precise micromechanisms of crack advance are presently unknown.

Despite the uncertainty in the mechanistic nature of ceramic fatigue, two general classes of mechanisms can be identified (where failure is associated with a dominant crack), specifically involving either *intrinsic* or *extrinsic* mechanisms;[4),12)] these are illustrated schematically in Fig. 11. Intrinsic mechanisms involve the actual creation of a fatigue-damaged microstructure ahead of the crack tip, and thus result in a crack-advance mechanism unique to cyclic fatigue. This could entail crack extension via alternating crack-tip blunting and re-sharpening, as in metals where the consequent striation fracture morphology is distinct from monotonic fracture modes, or through the formation of shear or tensile cracking at the tip due to contact between the mating fracture surfaces on unloading. In fact, fatigue striations have been reported for cyclic failure in zirconia ceramics.[10),11)] Another example is the high temperature fatigue of SiC-whisker-reinforced alumina; cyclic fractures show clear evidence of whisker breakage, whereas under quasi-static loads the majority of whiskers oxidize to form glass pockets.[32)]

Extrinsic mechanisms, conversely, do not necessarily involve a change in crack-advance mechanism compared to monotonic fracture; here, the role of the unloading cycle is to affect the magnitude of the *near-tip* stress intensity by diminishing the effect of crack-tip shielding. Several mechanisms are feasible. These include reduced

shielding through an enhanced forward transformation zone in transforming ceramics, although careful Raman spectroscopy measurements have not revealed any change in zone size in Mg-PSZ for cyclic and quasi-static conditions at the same K_{max}.[4),50)] An alternative mechanism is the reduction in crack-tip bridging via the cyclic induced failure of the bridges in the crack wake, where several possible processes exist. In ductile-particle toughened composites, cyclic loading may simply cause fatigue cracking in the ductile phase, which would otherwise remain intact under quasi-static loads and act as a crack bridge. An example of this is in γ-TiAl intermetallics reinforced with TiNb particles.[56)] Under monotonic loading, bridging zones of uncracked TiNb particles in excess of 3 mm are formed in the crack wake leading to an elevation in the fracture toughness K_c from 8 MPa$\sqrt{m}$ in unreinforced γ-TiAl to over 25 MPa$\sqrt{m}$ in the composite; under cyclic loading, conversely, the TiNb particles suffer fatigue failure to within ~150 μm of the crack tip, such that the ductile-particle bridging mechanism essentially is obliterated. Also it is feasible that brittle fibers or whiskers in specific composites may similarly fracture and/or buckle due to the unloading cycle, again diminishing shielding by crack bridging under cyclic loads. Finally, in certain monotonic ceramics, such as coarse-grained alumina, where toughening is achieved (primarily for intergranular fracture) by grain bridging or the interlocking of fracture-surface asperities between the crack faces,[57),58)] in cyclic fatigue, the unloading cycle may cause cracking and/or crushing of the asperities, or may degrade the grain-bridging mechanism through progressive wear of the sliding interfaces. In fact, evidence for the latter mechanism has recently been obtained in alumina using *in situ* scanning electron microscopy.[59)]

Indirect evidence for the extrinsic mechanism for cyclic fatigue-crack advance by the suppression of shielding can also be found from studies on small cracks in alumina and silicon nitride.[19),29)] In a comparison of cyclic and quasi-static behavior, small surface cracks, which because of their limited wake would have developed only minimal shielding, were found to show no acceleration under cyclic loading; long cracks, conversely, were found to be significantly accelerated by the cyclic loads, consistent with their higher shielding levels.[29)]

6. Design Considerations

For structural design where failure results from the propagation of a single dominant crack, cyclic fatigue in ceramic materials presents unique problems. In safety-critical applications involving metallic structures, damage-tolerant design and

life-prediction procedures generally rely on the integration of crack velocity/stress intensity (v/K) curves (e.g., Eq. 1) to estimate the time or number of cycles for a presumed initial defect to grow to critical size. Although such data are now available for many ceramic materials, the approach may prove difficult to utilize in practice because of the large power-law dependence of growth rates on stress intensity, which implies that the projected life will be proportional to the reciprocal of the applied stress raised to a large power.[8)]

For example, for a cracked structure subjected to an alternating stress $\Delta\sigma$, where the applied (far-field) stress-intensity factor K can be defined in terms of an applied stress σ and a geometry factor Q' as:

$$K = Q' \sigma\sqrt{(\pi a)} \ , \tag{7}$$

the projected number of cycles N_f to grow a crack from some initial size a_o to a critical size a_c is given by:

$$N_f = \frac{2}{(m-2)\, C(Q'\Delta\sigma)^m \, \pi^{(m/2)}} \left[a_o^{-\{(m-2)/2\}} - a_c^{-\{(m-2)/2\}}\right] \ , \tag{8}$$

assuming a crack-growth relationship of the form of Eq. 1 (for $m \neq 2$). For metallic structures where the exponent m is of the order of 2 to 4, a factor of two increase in the applied stress reduces the projected life by roughly an order of magnitude; in ceramic structures, conversely, where m values generally exceed 20 (and can be as high as 50 to 100), this same factor of two increase in stress reduces the projected life by some six to thirty orders of magnitude!

Thus, conventional damage-tolerant criteria for ceramics imply that marginal differences in the assumption of the component in-service stresses will lead to significant variations in projected life. Furthermore, any fluctuation of the applied stress and possible overloads frequently encountered in service may also result in highly non-conservative design lives. Two additional features of the approach provide further complication. First, in many practical applications, acceptable projected component life may only be guaranteed by restricting the initial defect size to extremely small sizes, often below the resolution of non-destructive evaluation techniques. Expensive and time consuming on-line scanning electron microscopy or proof testing at elevated loads of individual components are therefore required; in fact, these procedures are

currently in use in quality control procedures for pyrolytic-carbon prosthetic heart-valve devices. Second, and perhaps most important, the approach generally does not consider, and in this case cannot easily be modified to include, small-crack effects such as those described above.

An alternative procedure is to redefine the critical crack size in terms of the fatigue threshold, ΔK_{TH}, below which crack growth is presumed dormant; this in essence is a crack-initiation criterion where ΔK_{TH} is taken as the effective toughness, rather than the fracture toughness K_c. This procedure, in addition to sharing similar problems associated with defining a minimum detectable defect size, also does not address small-crack effects which may arise at loads considerably below those required for the growth of long-cracks. As a result, although data on the small-crack effect in ceramic fatigue are very limited, the observed sub-threshold crack-growth behavior implies that conventional damage-tolerant design criteria may be again highly non-conservative for ceramics.

Like many high strength metallic materials, however, crack-initiation effects may involve a very significant portion of lifetime under alternating loads. Having referred to a number of potential limitations of a fracture-mechanics approach to ensure component reliability, it is important to note that these approaches are typically highly conservative in the sense that they assume crack growth from the first loading cycle. Although the degree of this conservatism is difficult to quantify, due in part to the paucity of data from crack-initiation studies, the disadvantages of the approach may in fact be considerably outweighed by neglecting the cycles required for initiation. Selection of a damage-tolerant approach is, therefore, at present undertaken on a case by case basis, often affected by the requirements of appropriate regulatory agencies.

The importance of fatigue-crack initiation does, however, suggest an additional design criterion for ceramic components; this more traditional approach is invariably based on stress/life S/N data. In addition to simple consideration of the fatigue limit, a more sophisticated approach might include a damage-mechanics analysis utilizing detailed finite-element stress analyses for components of complex shape and a statistical evaluation of the pre-existing defect population. While this approach has serious limitations in some applications, particularly in large structures where numerous defects may be present and therefore fatigue-crack initiation periods diminished, it might be quite appropriate for small ceramic components. Clearly, more indepth studies of both fatigue-crack initiation and crack-growth behavior, together with improved design criterion are required to enhance the in-service reliability and life prediction of ceramic and ceramic-matrix components subjected to alternating loads.

7. Conclusions

1. Results on a wide range of monolithic and composite ceramics clearly indicate a strong susceptibility to mechanical degradation under cyclic loading. Ceramic fatigue is promoted by inelastic deformation mechanisms, such as microcracking and transformation "plasticity" in monolithic ceramics and irreversible deformation in the reinforcement phase or its interface with the matrix in composites.

2. Stress/life (S/N) data show lifetimes to be shorter under cyclic loading compared to corresponding lifetimes under quasi-static (static fatigue) loading at the same maximum stress. In many ceramics, "fatigue limits" at 10^8 cycles ($R = -1$) approach ~50% of the single-cycle tensile (or bending) strength. Data on unnotched samples indicate that cycling in tension-compression ($R = -1$) is generally more damaging that in tension-tension ($R > 0$).

3. With the exception of SiC, cyclic fatigue lifetimes in S/N tests at ambient temperatures are less than those predicted from static fatigue data assuming only time-dependent (and not cycle-dependent) processes; conversely, at high homologous temperatures, results for alumina at 1200°C suggest that the reverse is true.

4. Cyclic fatigue-crack growth rates for long (>3 mm) cracks are found to be power-law dependent on the applied stress intensity (ΔK, K_{max}), with an exponent m much larger than typically observed for metals (i.e., in the range ~10 to over 100). Crack-growth behavior is sensitive to several factors including microstructure, load ratio, environment and crack size. Fatigue threshold stress intensities (ΔK_{TH}), below which long cracks are presumed dormant, approach ~50% of the fracture toughness (K_c).

5. At ambient temperatures, crack-growth rates under cyclic loading generally exceed those by static fatigue (at the same K_{max}) by many orders of magnitude. Conversely, at high homologous temperatures (1000° to 1400°C) in the creep regime, cyclic fatigue-crack growth rates in monolithic and SiC_w-reinforced alumina have been observed to be less than those measured under quasi-static loads.

6. Cyclic fatigue-crack growth rates for small (<250 μm) surface cracks are found to be in excess of corresponding long cracks at the same applied stress intensity, and furthermore to occur at stress intensities significantly smaller than the nominal long-crack threshold, ΔK_{TH}. Similar to metallic materials, small-crack growth rates show a negative dependency on applied stress intensity and appear sensitive to the applied stress level. Such behavior is attributed to diminished crack-tip shielding (e.g.,

by transformation toughening in Mg-PSZ or crack bridging in whisker- or fiber-reinforced composites) with cracks of limited wake.

7. The fractography of failures by cyclic fatigue is frequently similar and often indistinguishable from corresponding failures under quasi-static loading. Such similarity complicates the post-fracture failure analysis of ceramic components.

8. Although precise micro-mechanisms of cyclic fatigue are currently uncertain, two classes are identified. *Intrinsic* mechanisms involve the creation of an inherent fatigue-damaged microstructure ahead of the crack tip and hence result in a crack-advance mechanism unique to cycle fatigue (as in metals). *Extrinsic* mechanisms involve no change in crack-advance mechanism compared to that under quasi-static loading; here the unloading cycle acts to enhance the near-tip stress intensity by diminishing the role of crack-tip shielding.

9. Cyclic fatigue-crack growth-rate data, particularly pertaining to small cracks, have significant implications for damage-tolerant lifetime prediction and design criteria in ceramic materials. The observed marked dependency of growth rates on the stress intensity implies an excessive dependency of projected lifetime on applied stress; this leads to difficulties in applying conventional damage-tolerant procedures. An indepth understanding of the initiation and growth of microstructurally-small cracks is required to provide more reliable design criteria for safety-critical applications.

Acknowledgments The work on monolithic ceramics was supported by the Director, Office of Energy Research, Office of Basic Energy Sciences, Materials Sciences Division of the U.S. Department of Energy under Contract No. DE-AC03-76SF00098; research on composite ceramics was funded by the Office of Naval Research under Grant No. N00014-89-J-1094.

References

1) R. H. Dauskardt, W. Yu and R. O. Ritchie, *J. Am. Ceram. Soc.*, **70**, 248-52 (1987).

2) M. V. Swain and V. Zelizko, pp. 595-606 in *Advances in Ceramics, 24B Science and Technology of Zirconia III*, Edited by S. Somioya, N. Yammoto and H. Hanagida, American Ceramic Society, Westerville, OH, 1988.

3) L. A. Sylva and S. Suresh, *J. Mater. Sci.*, **24**, 1729-38 (1989).

4) R. H. Dauskardt, D. B. Marshall and R. O. Ritchie, *J. Am. Ceram. Soc.*, **73**, 893-903 (1990).

5) R. H. Dauskardt, W. C. Carter, D. K. Veirs and R. O. Ritchie, *Acta Metall. Mater.*, **38**, 2327-36 (1990).

6) T. Kawakubo, N. Okabe and T. Mori, pp 717-32 in *Fatigue '90* (Proc. 4th Intl. Conf. on Fatigue and Fatigue Thresholds), Vol. 2, Edited by H. Kitagawa and T. Tanaka, Mat. Comp. Eng. Publ., Ltd., Edgbaston, U.K., 1990.

7) A. A. Steffen, R. H. Dauskardt and R. O. Ritchie, pp. 745-52 in *Fatigue '90* (Proc. 4th Intl. Conf. on Fatigue and Fatigue Thresholds), Vol. 2, Edited by H. Kitagawa and T. Tanaka, Mat. Comp. Eng. Publ., Ltd., Edgbaston, U.K., 1990.

8) A. A. Steffen, R. H. Dauskardt and R. O Ritchie, *J. Am. Ceram. Soc.*, **74**, (1991) in press.

9) D. C. Cardona and C. J. Beevers, pp. 1023-29 in *Fatigue '90* (Proc. 4th Intl. Conf. on Fatigue and Fatigue Thresholds), Vol. 2, Edited by H. Kitagawa and T. Tanaka, Mat. Comp. Eng. Publ., Ltd., Edgbaston, U.K., 1990.

10) S.-Y. Liu and I.-W. Chen, *J. Am. Ceram. Soc.*, **74**, (1991) in press.

11) D. L. Davidson, J. B. Campbell and J. Lankford, J., *Acta Metall. Mater.*, **39**, (1991) in review.

12) R. O. Ritchie, R. H. Dauskardt, W. Yu and A. M. Brendzel, *J. Biomed. Mater. Res.*, **24**, 189-206 (1990).

13) F. Guiu, *J. Mater. Sci. Lett.*, **13**, 1357-61 (1978).

14) H. N. Ko, *J. Mater. Sci. Lett.*, **5**, 464-66 (1986).

15) L. Ewart and S. Suresh, *J. Mater. Sci. Lett.*, **5**, 774-78 (1986).

16) T. Hoshide, T. Ohara and T. Yamada, *Int. J. Fracture*, **37**, 47-59 (1988).

17) G. Grathwohl and T. Liu, *J. Am. Ceram. Soc.*, **72**, 1988-90 (1989).

18) H. N. Ko. *J. Mater. Sci. Lett.*, **8**, 1438-41 (1989).

19) S. Lathabai, Y.-W. Mai and B. R. Lawn, *J. Am. Ceram. Soc.*, **72**, 1760-63 (1989).

20) M. J. Reece, F. Guiu and M. F. R. Sammur, *J. Am. Ceram. Soc.*, **72**, 348-52 (1989).

21) I. Bar-On and J. T. Beals, pp. 793-98 in *Fatigue '90* (Proc. 4th Intl. Conf. on Fatigue and Fatigue Thresholds), Vol. 2, Edited by H. Kitagawa and T. Tanaka, Mat. Comp. Eng. Publ., Ltd., Edgbaston, U.K., 1990..

22) C.-K. J. Lin and D. F. Socie, *J. Am. Ceram. Soc.*, **74**, (1991) in press.

23) T. Fett, G. Martin, D. Munz and G. Thun, *J. Mater. Sci.*, (1991) in press.

24) T. Fett and D. Munz, Proc. 7th World Ceramics Congress (CIMTEC), Montecatini Therme, Italy, 1990, in press.

25) T. Kawakubo and K. Komeya, *J. Am. Ceram. Soc.*, **70**, 400-05 (1987).

26) S. Horibe, *J. Mater. Sci. Lett.*, **7**, 725-27 (1988).

27) M. Masuda, T. Soma, M. Matsui and I. Oda, *J. Ceram. Soc. Japan Inter. Ed.*, **96**, 275-80 (1988).

28) A. Ueno, H. Kishimoto, H. Kawamoto and M. Asakwa, pp. 733-38 in *Fatigue '90* (Proc. 4th Intl. Conf. on Fatigue and Fatigue Thresholds), Vol. 2, Edited by H. Kitagawa and T. Tanaka, Mat. Comp. Eng. Publ., Ltd., Edgbaston, U.K., 1990.

29) Y. Mutoh, M. Takahashi, T. Oikawa and H. Okamoto, in *Fatigue of Advanced Materials*, Edited by R. O. Ritchie, R. H. Dauskardt, and B. N. Cox, Mat. Comp. Eng. Publ., Ltd., Edgbaston, U.K., 1991.

30) S. Lauf, V. Gerold and R. F. Pabst, pp. 775-80 in *Fatigue '90* (Proc. 4th Intl. Conf. on Fatigue and Fatigue Thresholds), Vol. 2, Edited by H. Kitagawa and T. Tanaka, Mat. Comp. Eng. Publ., Ltd., Edgbaston, U.K., 1990.

31) E. H. Luh, R. H. Dauskardt and R. O. Ritchie, *J. Mater. Sci. Lett.*, **9**, 719-25 (1990).

32) L. X. Han and S. Suresh, *J. Am. Ceram. Soc.*, **72**, 1233-38 (1989).

33) R. H. Dauskardt, M. R. James, J. R. Porter and R. O. Ritchie, *J. Am. Ceram. Soc.*, **74**, (1991) in review.

34) J. W. Holmes, *J. Am. Ceram. Soc.*, **74**, (1991) in press.

35) R. O. Ritchie, *Int. Met. Rev.*, **20**, 205-30 (1979).

36) R. O. Ritchie and W. Yu, pp. 167-89 in *Small Fatigue Cracks*, Edited by R. O. Ritchie and J. Lankford, The Metallurgical Society of the American Institute of Mining, Metallurgical, and Petroleum Engineers, Warrendale, PA, 1986.

37) P. C. Paris and F. Erdogan, *J. Bas. Eng.*, Trans. ASME, **85**, 528-34 (1963).

38) S. Suresh and R. O. Ritchie, *Intl. Metals Rev.*, **29**, 445-76 (1984).

39) H. Tada, P. C. Paris and G. R. Irwin, *Stress Analysis of Cracks Handbook*, Paris Publications Inc./Del Research Corp., St. Louis, MO, 1985.

40) J. C. Newman, Jr. and I. S. Raju, pp. 312-34 in *Computational Methods in the Mechanics of Fracture*, Chapter 9, Vol. 2, Edited by S. N. Atluri, North Holland, Amsterdam, 1986.

41) R. W. Hertzberg, W. A. Herman and R. O. Ritchie, *Scripta Metall.*, **21**, 1541-46 (1987).

42) W. Elber, pp. 230-42 in *Damage Tolerance in Aircraft Structures*, ASTM STP 486, American Society for Testing and Materials, Philadelphia, PA, 1971.

43) S. Suresh and R. O. Ritchie, pp. 227-61 in *Fatigue Crack Growth Threshold Concepts*, Edited by D. L. Davidson and R. O. Ritchie, The Metallurgical Society of the American Institute of Mining, Metallurgical, and Petroleum Engineers, Warrendale, PA, 1984.

44) R. H. J. Hannick and M. V. Swain, *J. Aust. Ceram. Soc.*, **18**, 53-62 (1982).

45) R. H. J. Hannick, *J. Mater. Sci.*, **18**, 457-70 (1983).

46) D. B. Marshall, *J. Am. Ceram. Soc.*, **69**, 173-88 (1986).

47) R. M. McMeeking and A. G. Evans, *J. Am. Ceram. Soc.*, **63**, 242-46 (1982).

48) B. Budiansky, J. W. Hutchinson and J. C. Lambropoulos, *Int. J. Solids Struct.*, **19**, 337-55 (1983).

49) R. H. Dauskardt, D. K. Veirs and R. O. Ritchie, *J. Am. Ceram. Soc.*, **72**, 1124-30 (1989).

50) D. B. Marshall, M. C. Shaw, R. H. Dauskardt, R. O. Ritchie, M. Readey and A. H. Heuer, *J. Am. Ceram. Soc.*, **73**, 2659-66 (1990).

51) R. O. Ritchie, R. H. Dauskardt and F. J. Pennisi, *J. Biomed. Mater. Res.*, **25**, (1991) in review.

52) R. W. Hertzberg, *Deformation and Fracture Mechanics of Engineering Materials*, 3rd ed., Wiley, New York, NY, 1989.

53) T. Fett, G. Himsolt and D. Munz, *Adv. Ceram. Matls.*, **1**, 179-84 (1986).

54) P. Neumann, *Acta Metall.*, **22**, 1155-65 (1974).

55) A. G. Evans, pp. 267-91 in *Fracture Mechanics: Perspectives and Directions (Twentieth Symp.)*, ASTM STP 1020, Edited by R. P. Wei and R. P. Gangloff, American Society for Testing and Materials, Philadelphia, PA, 1989.

56) K. T. Venkateswara Rao, G. R. Odette and R. O. Ritchie, *Acta Metall. Mater.*, **39**, (1991) in review.

57) P. L. Swanson, C. J. Fairbanks, B. R. Lawn, Y.-W. Mai and B. J. Hockey, *J. Am. Ceram. Soc.*, **70**, 279-89 (1987).

58) G. Vekinis, M. F. Ashby and P. W. R. Beaumont, *Acta Metall. Mater.* **38**, 1151-62 (1990).

59) S. Lathabai, J. Rödel and B. R. Lawn, *J. Am. Ceram. Soc.*, **74**, (1991) in review.

Table 1 - Values of Parameters for S/N and Crack-Propagation Fatigue Tests for Ceramic Materials at Ambient Temperatures

		S/N	Crack Propagation (R = 0)			Ref.
	K_c (MPa$\sqrt{m}$)	slope n	C (m/c (MPa$\sqrt{m}$)$^{-m}$) (Eq.1)	slope m	ΔK_{TH} (MPa$\sqrt{m}$)	
alumina	~4.0	12.7-64	-	27-33	2.5-2.7	18,20
Mg-PSZ (TS-grade)	16.0	34	1.70×10^{-48}	42	7.7	4
(MS-grade)	11.5	36	5.70×10^{-28}	24	5.2	4
(AF-grade)	5.5	-	4.89×10^{-22}	24	3.0	1,4
(overaged)	2.9	-	2.00×10^{-14}	21	1.6	4
silicon nitride	6.0	~30	1.01×10^{-21}	12-18	2.0-4.3	21
3Y-TZP	5.3	~21	4.06×10^{-18}	21	2.4	10
Al_2O_3-SiC_w	4.5	-	3.28×10^{-20}	15	3.1	33
graphite/pyrolytic C	~1.6	-	1.86×10^{-18}	19	~0.7	12

Table 2 - Comparison of Fatigue Lifetimes at Various Load Ratios for Al_2O_3/SiC_w Composite

Load Ratio ($\sigma_{min}/\sigma_{max}$)	σ_{max} (MPa$\sqrt{m}$)	Life, N_f (cycles)
0.05	245	60×10^3
0.05	247	140×10^3
0.05	252	150×10^3
-1.0	248	60×10^3
-1.0	255	240×10^3

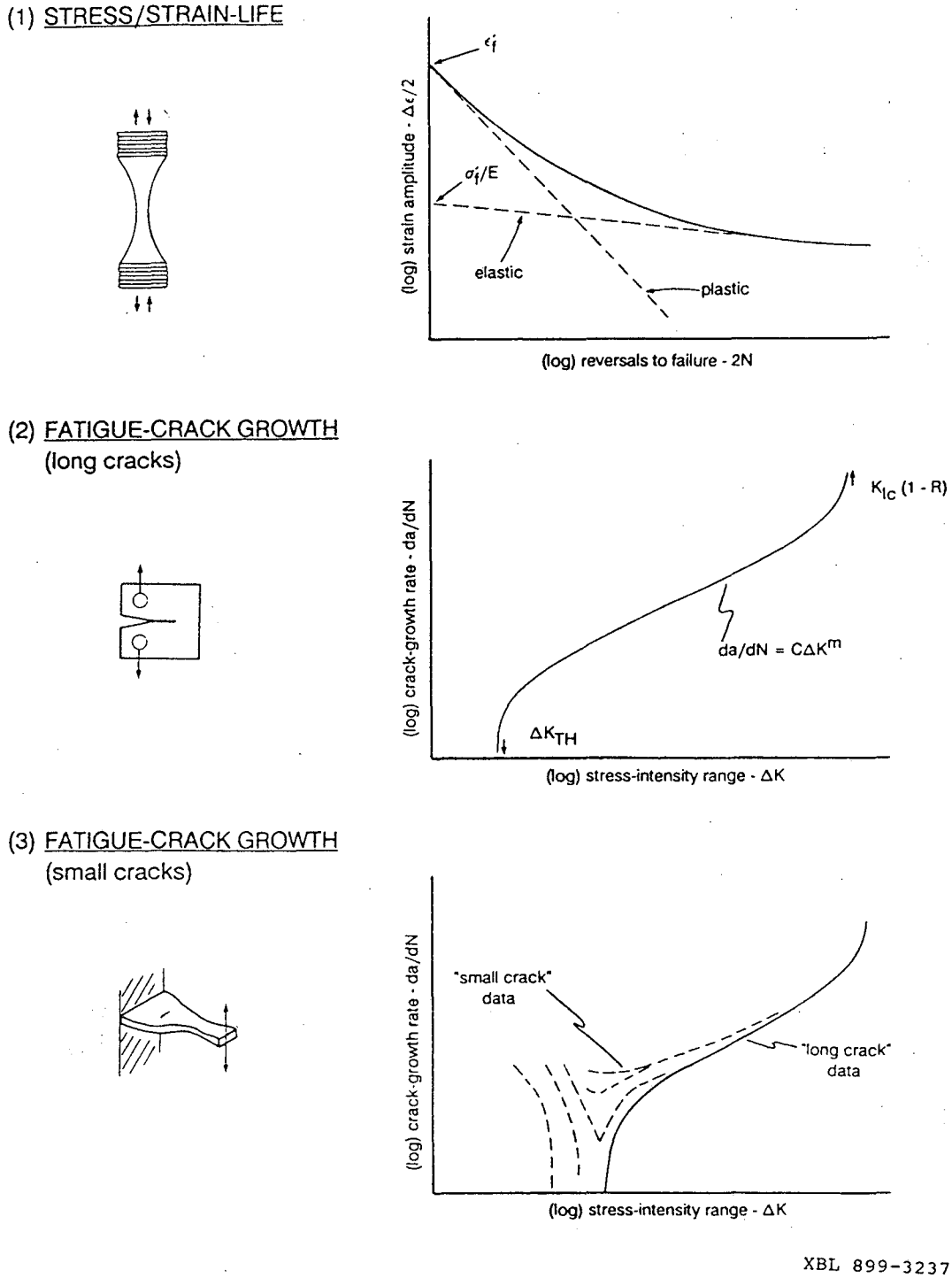

Figure 1: Methodologies for characterizing cyclic fatigue resistance in materials; a) stress or strain/life (S/N) testing, b) fatigue-crack propagation tests on long cracks (typically larger than ~3 mm), and c) fatigue-crack propagation testing on small cracks (typically ~1 to 250 μm in size).

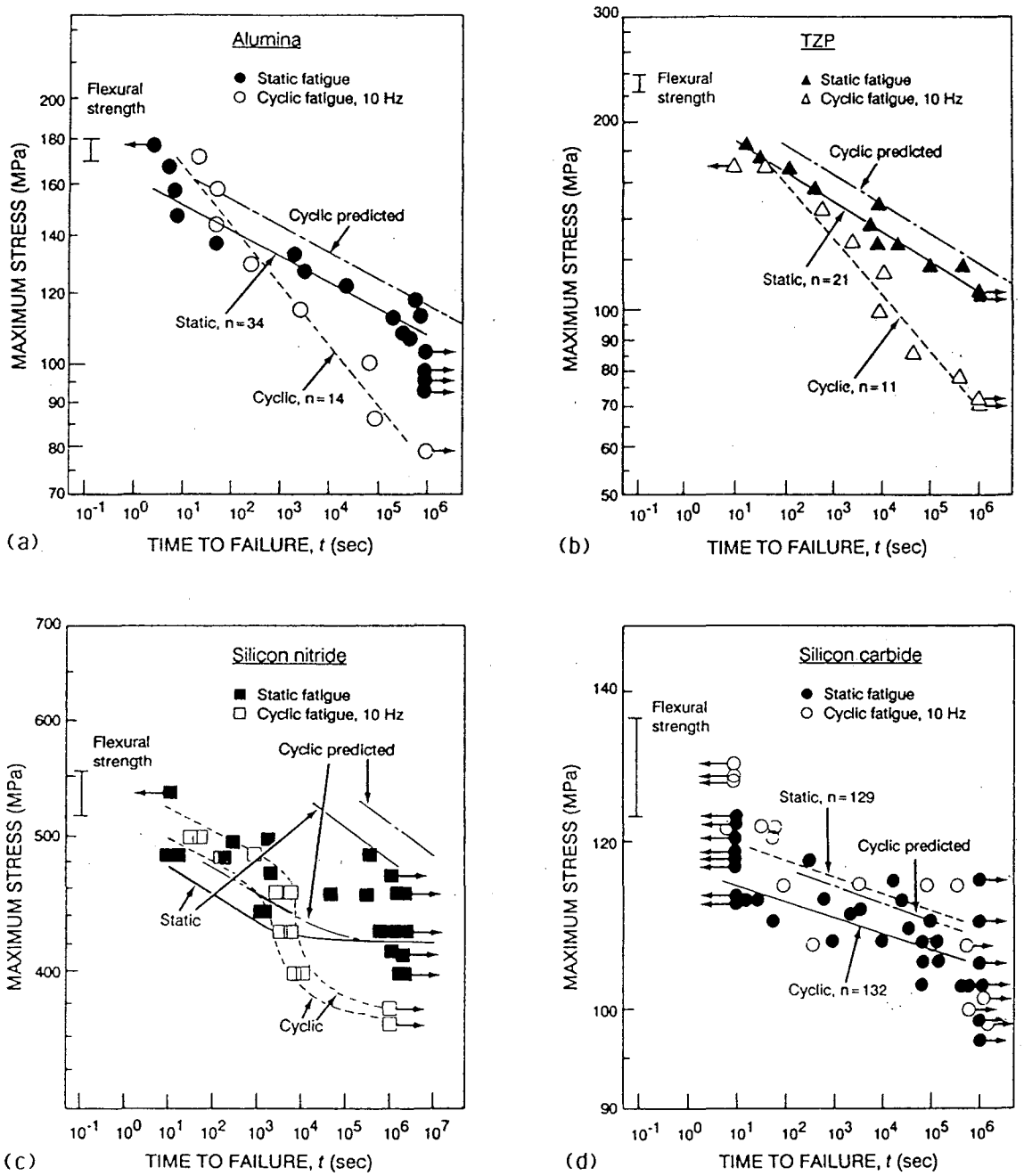

Figure 2: Comparison of stress/life results for a) alumina, b) TZP, c) silicon nitride, and d) silicon carbide under cyclic and quasi-static loading at ambient temperature. Four-point bend (R = 0) data from ref. 6.

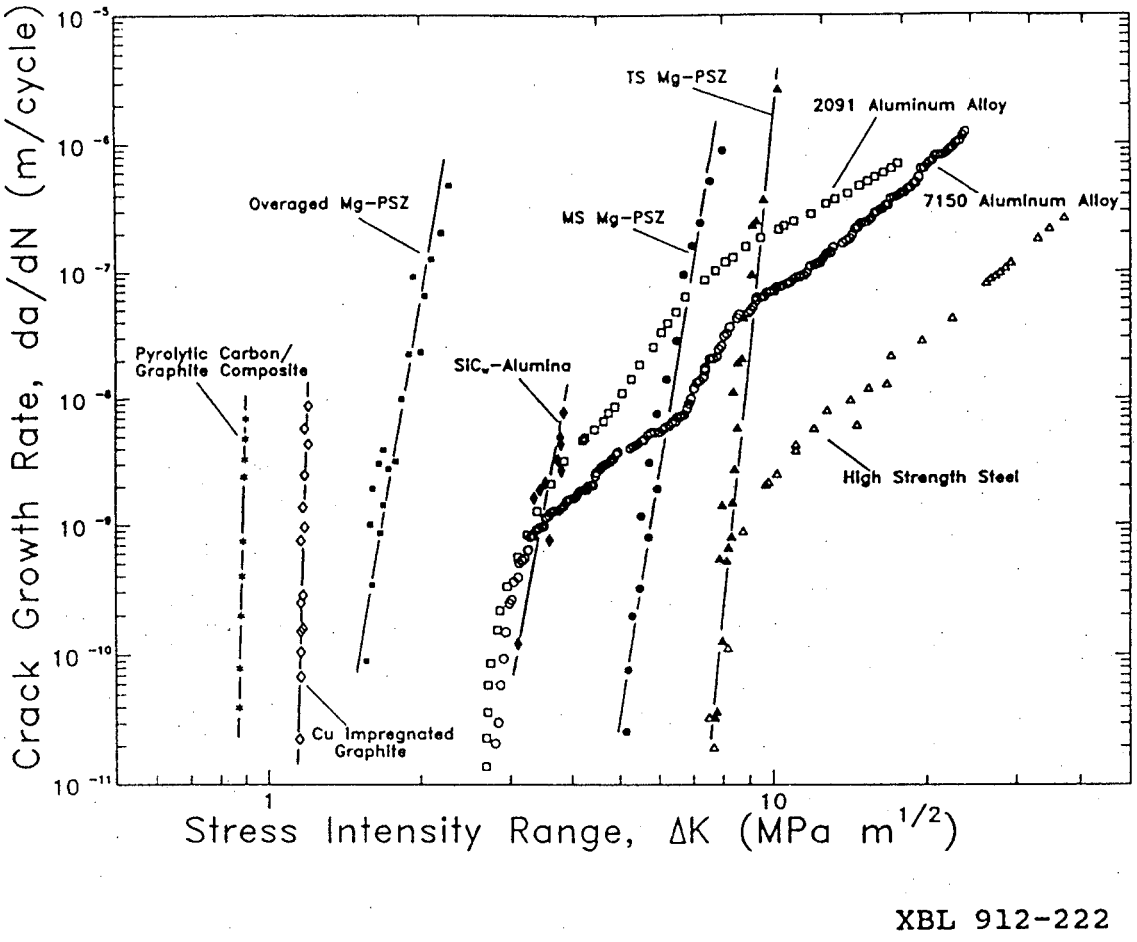

Figure 3: Cyclic fatigue-crack propagation behavior for a range of ceramics, namely, Mg-PSZ,[1),4)] pyrolytic carbon,[12)] Cu-impregnated graphite, and SiC-reinforced alumina;[33)] data are compared with three high-strength steel and aluminum metallic alloys.[35),36)]

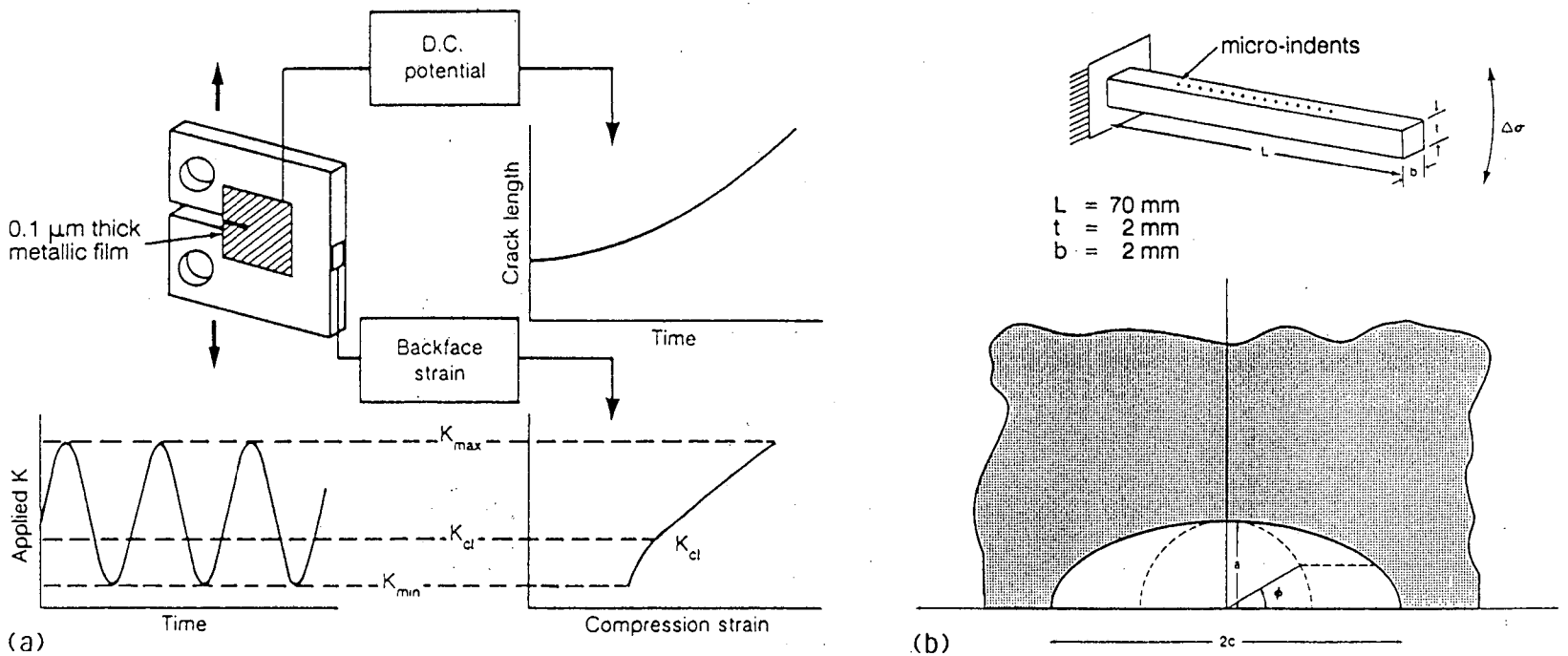

Figure 4: Experimental techniques used to measure cyclic fatigue-crack growth rates, showing a) compact tension C(T) specimen and procedures used to monitor crack length and the stress intensity, K_{cl}, at crack closure for long cracks, and b) cantilever-bend specimen and semi-elliptical surface crack configuration for tests on small cracks.[4),8),33)]

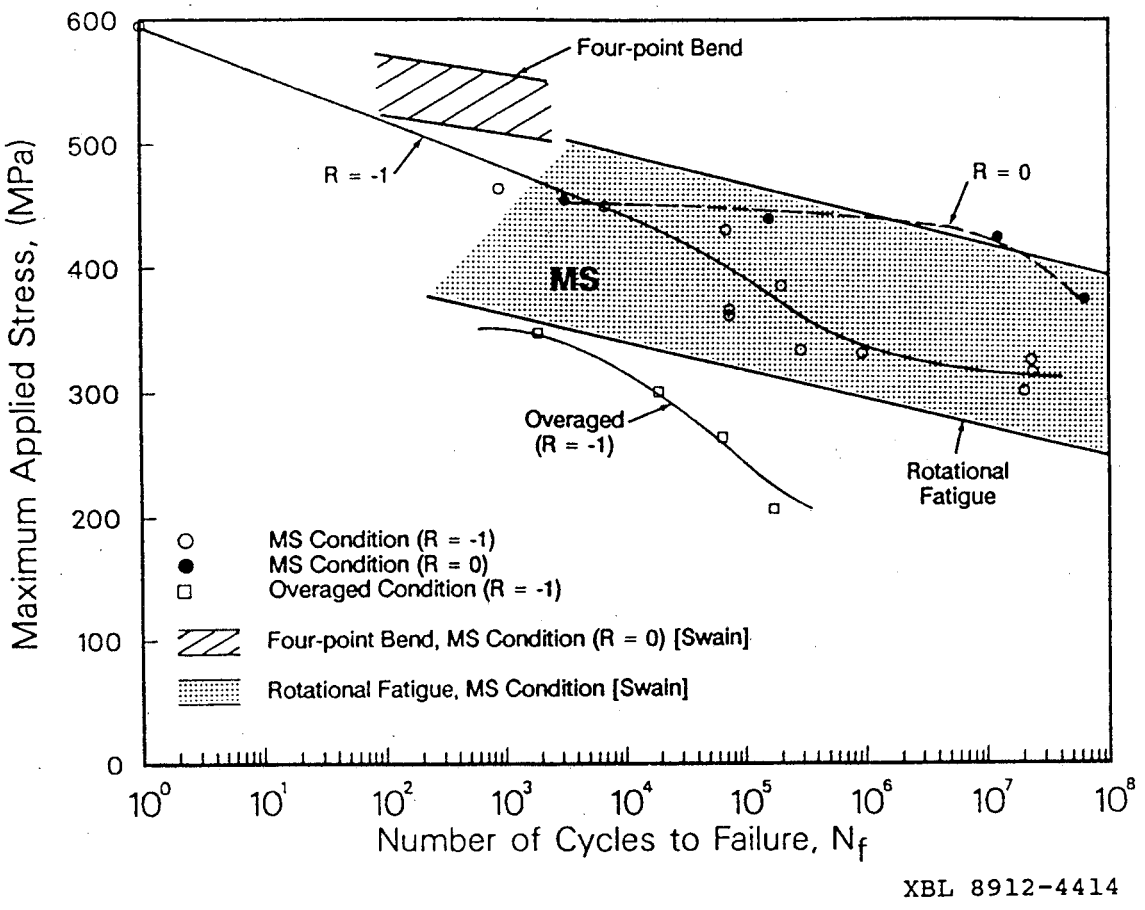

Figure 5: Stress/life (S/N) curves for the overaged and MS-grade Mg-PSZ tested in cantilever bend under tension-compression (R = -1) and tension-tension (R = 0) cycling.[7),8)] Data are compared with results of Swain and Zelizko[2)] on a similar MS-grade Mg-PSZ material under flexural bending (R = 0) and rotating bending (R = -1).

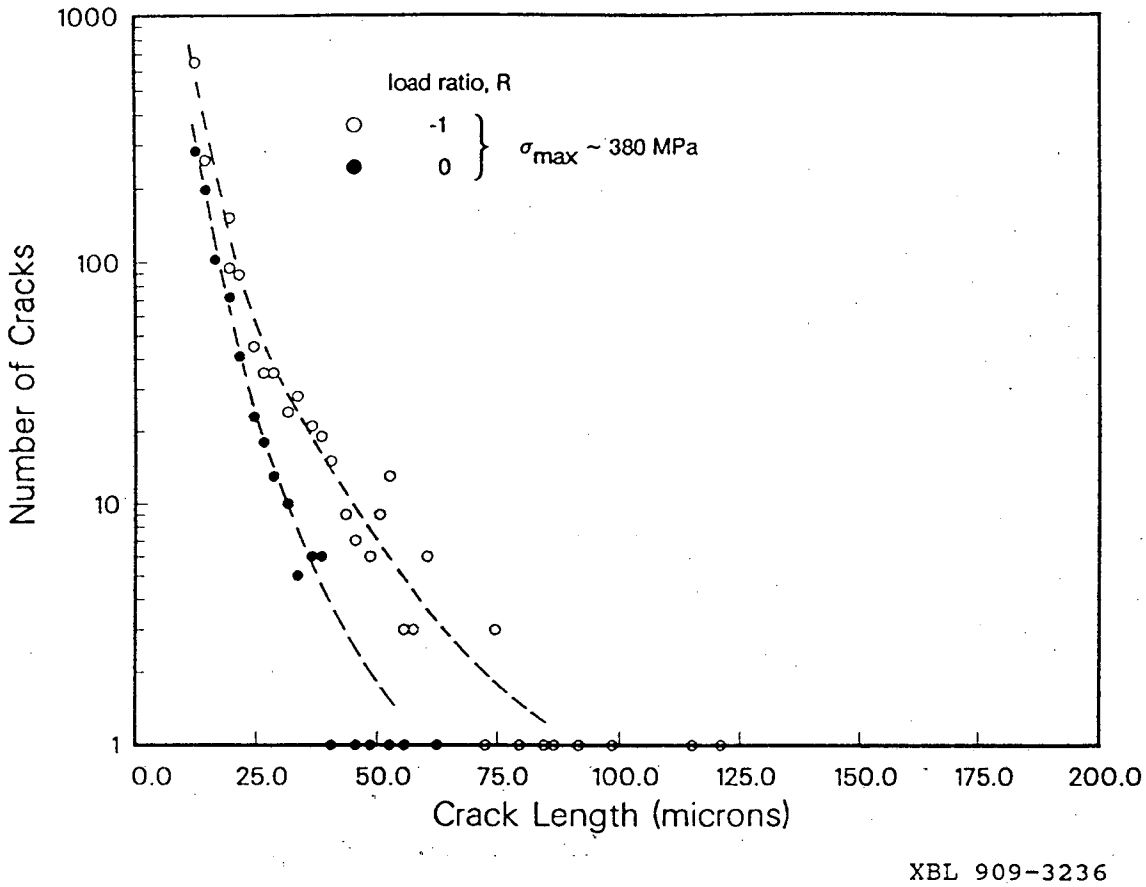

Figure 6: Microcrack size distributions for MS-grade Mg-PSZ measured on the surface of unnotched cantilever-bend specimens at a maximum alternating stress of ~380 MPa for both tension-compression and tension-tension loading.[8)]

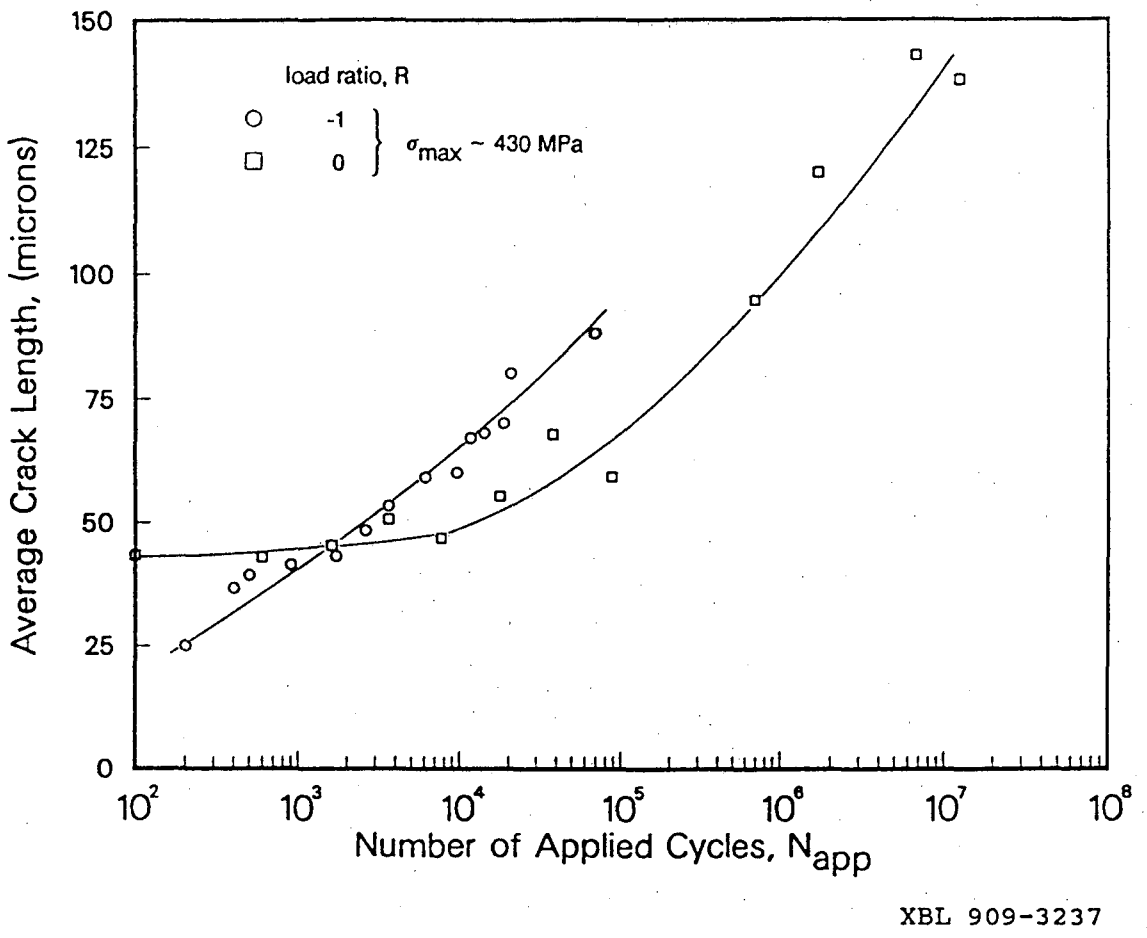

Figure 7: Surface crack length vs. number of cycles for small-crack growth at similar applied stress levels in unnotched cantilever-bend specimens of MS-grade Mg-PSZ tested at R = 0 and R = -1.[8)]

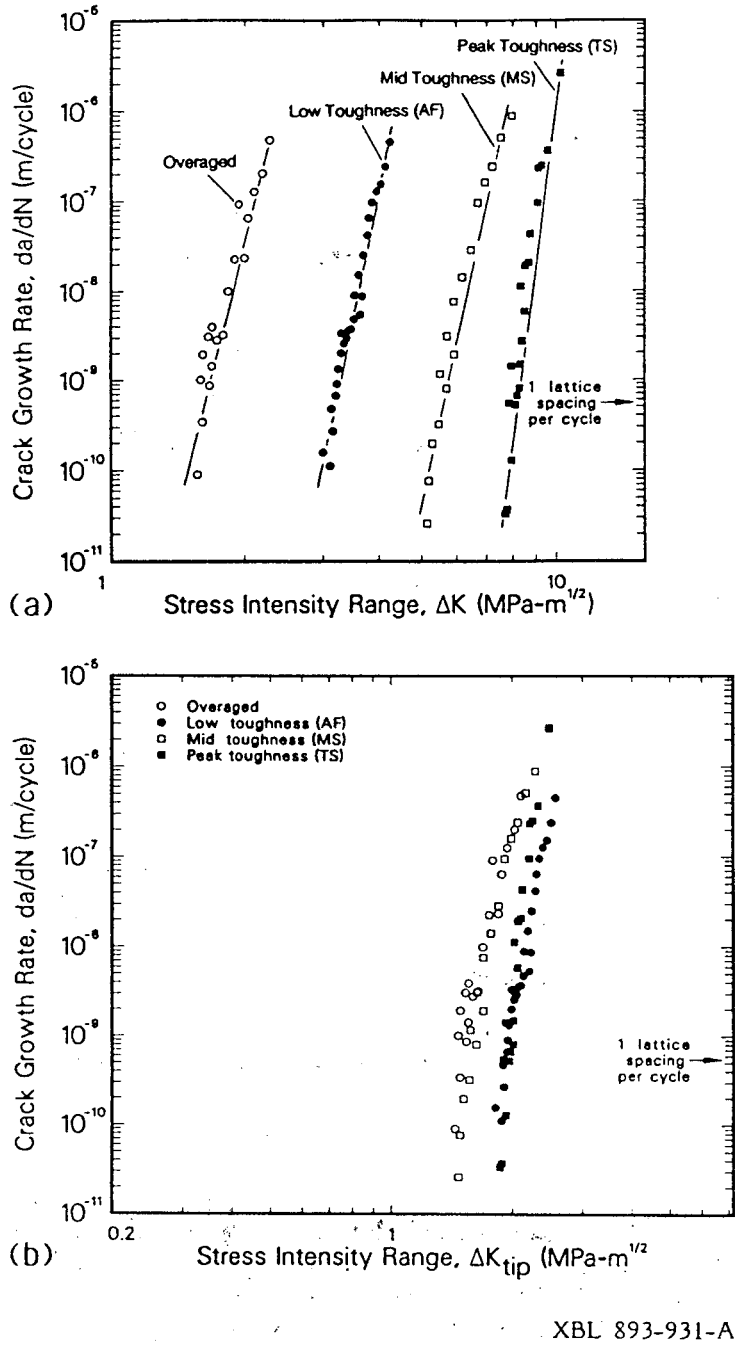

Figure 8: Long-crack growth-rate data in overaged and transformation-toughened Mg-PSZ, derived from C(T) specimens, as a function of a) nominal (applied) stress-intensity range, ΔK, and b) near-tip stress-intensity range, $\Delta K_{tip} = K_{max} - K_s$, showing that cyclic crack-growth resistance is increased with the degree of transformation toughening.[4)]

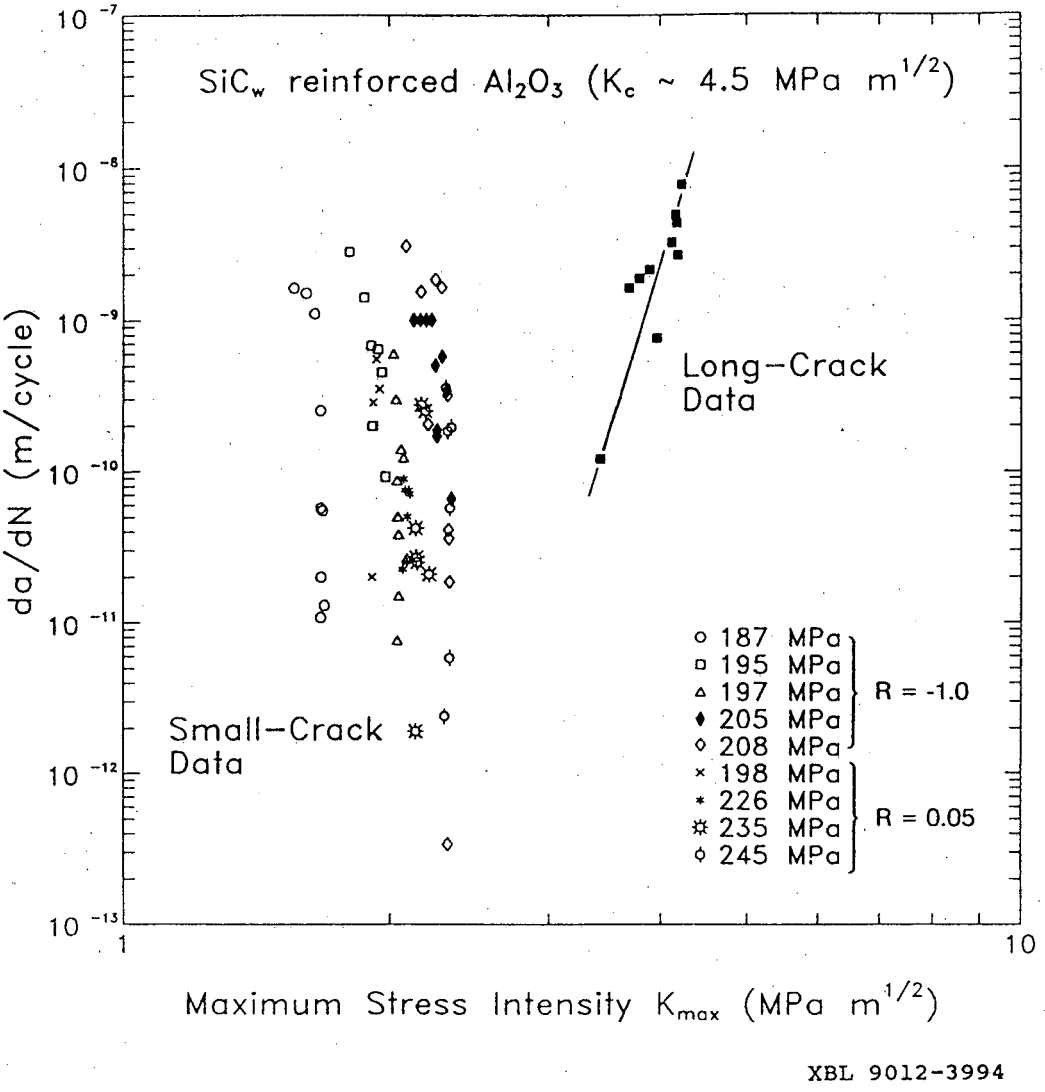

Figure 9: Small-crack growth-rate data in the Al_2O_3-SiC_w composite, derived from cantilever-bend specimens, as a function of K_{max} at R = 0.05 and -1, compared to corresponding long-crack data derived from C(T) specimens. Note how small cracks propagate at stress-intensity levels well below the long-crack threshold, ΔK_{TH}, and show a general negative dependency on applied stress intensity.[33]

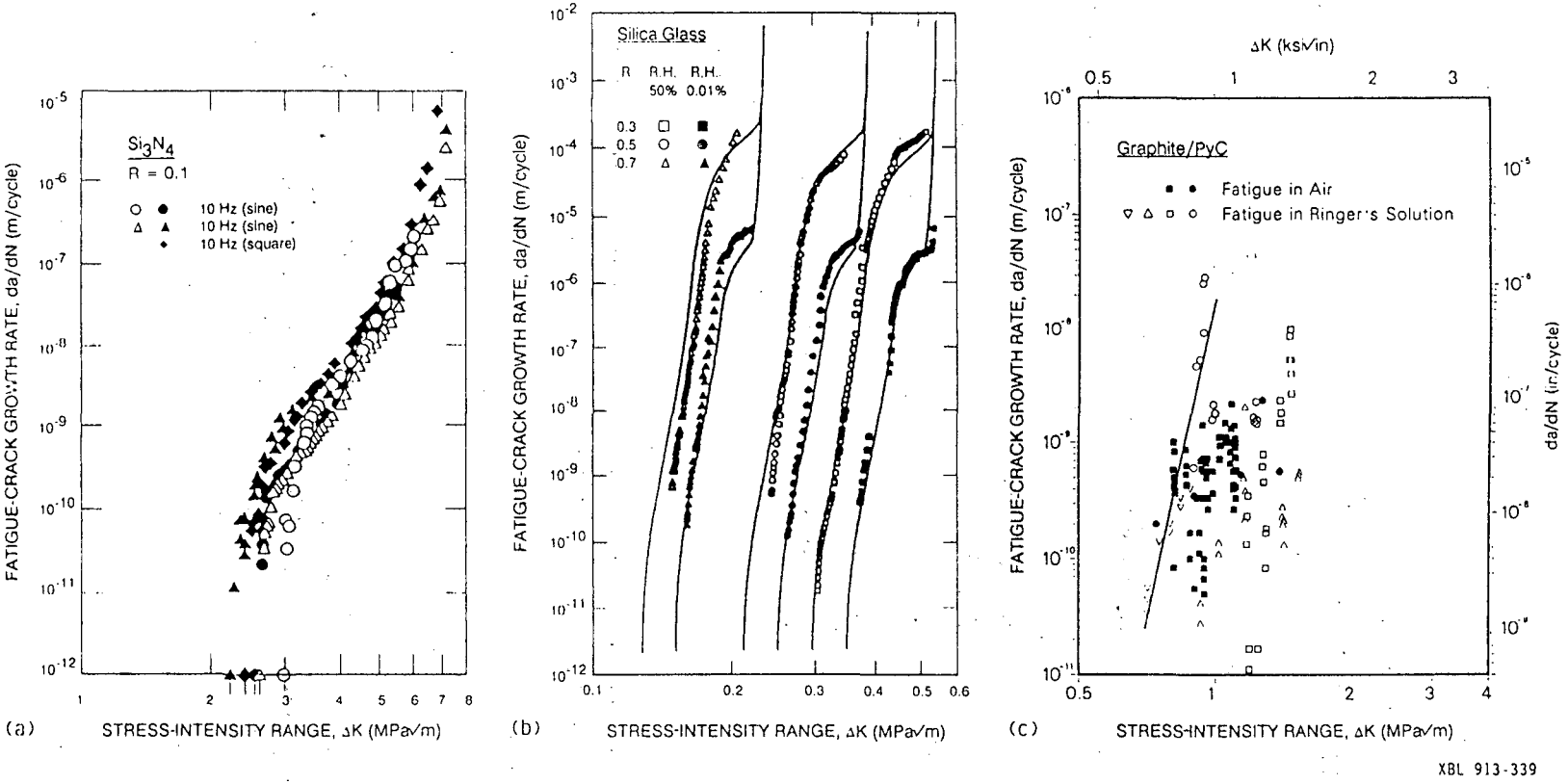

Figure 10: Cyclic fatigue-crack propagation results for a) silicon nitride,[29] b) silica glass,[30] and a pyrolytic-carbon coated graphite laminate.[12]

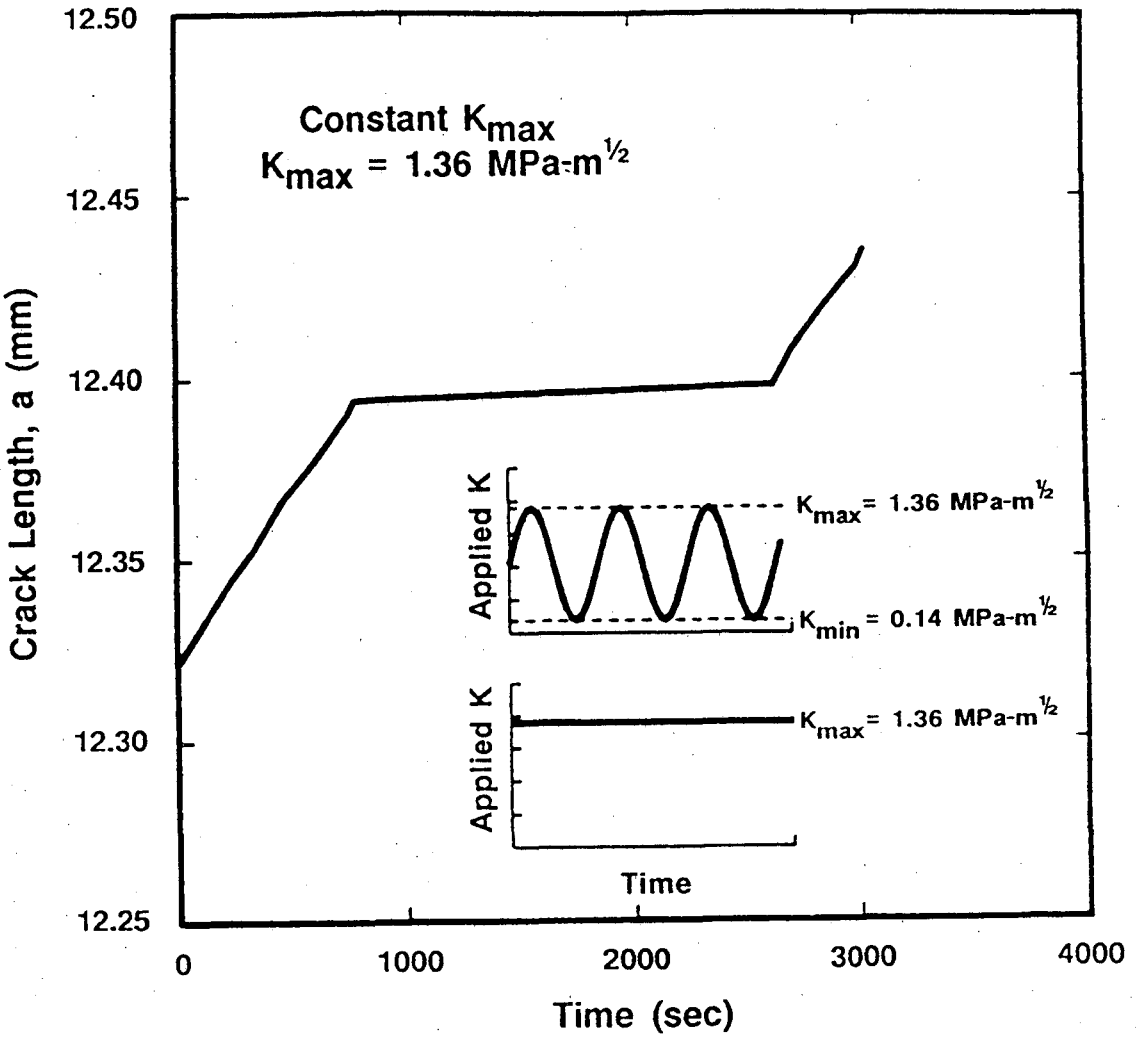

Figure 11: Effect of sustained-load vs. cyclic loading conditions, at a constant K_{max}, on subcritical crack growth in pyrolytic-carbon coated graphite tested at R = 0.1 (50 Hz) in Ringer's solution at 37°C (blood analog). Note how crack-growth rates under cyclic loading are far in excess of those measured under sustained (quasi-static) loading.[12]

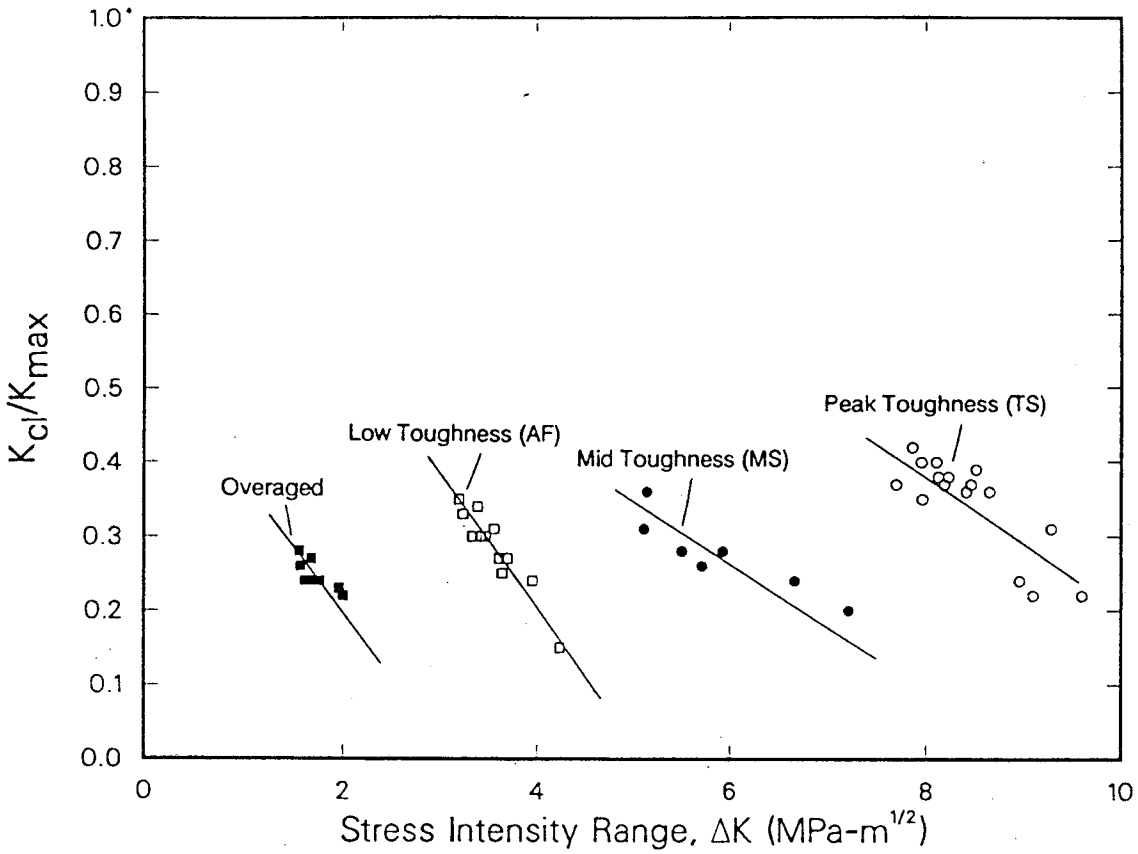

Figure 12: Experimentally measured variation in fatigue crack closure corresponding to cyclic crack-growth rate data at R = 0.1 for the Mg-PSZ microstructures plotted in Fig. 8. Results are based on back-face strain compliance measurements and show the ratio K_{cl}/K_{max} as a function of the applied stress-intensity range, ΔK.[4)]

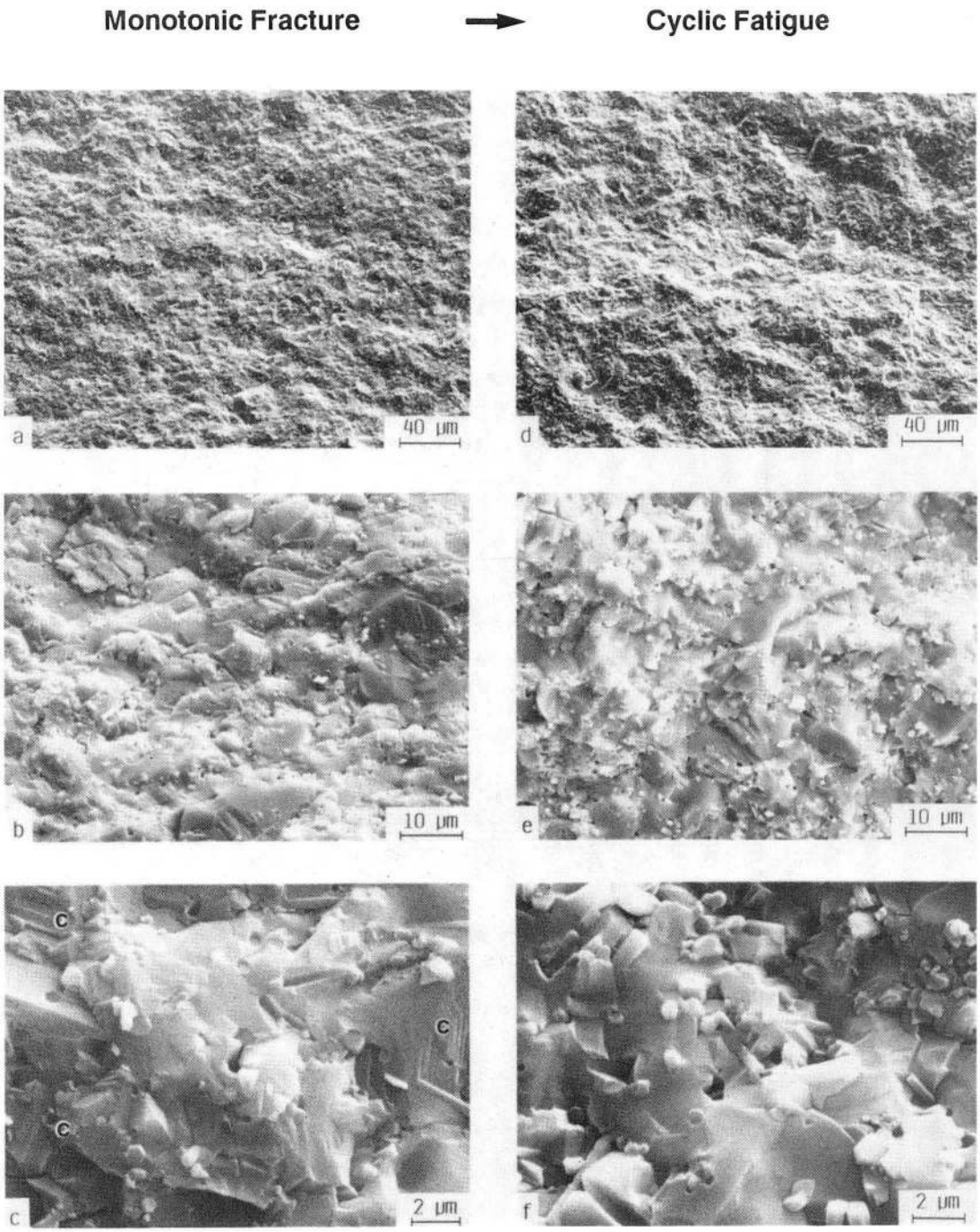

Figure 13: Scanning electron micrographs at increasing magnification of a,b,c) monotonic fracture and c,d,e) cyclic fatigue fracture in a SiC-whisker-reinforced alumina composite, showing the predominantly transgranular nature of crack paths and regions of cleavage-like steps (indicated by letter C) formed under quasi-static loading, compared to the rougher more intergranular fracture surfaces induced by cyclic loading. Horizontal arrow indicates direction of crack growth.[33]

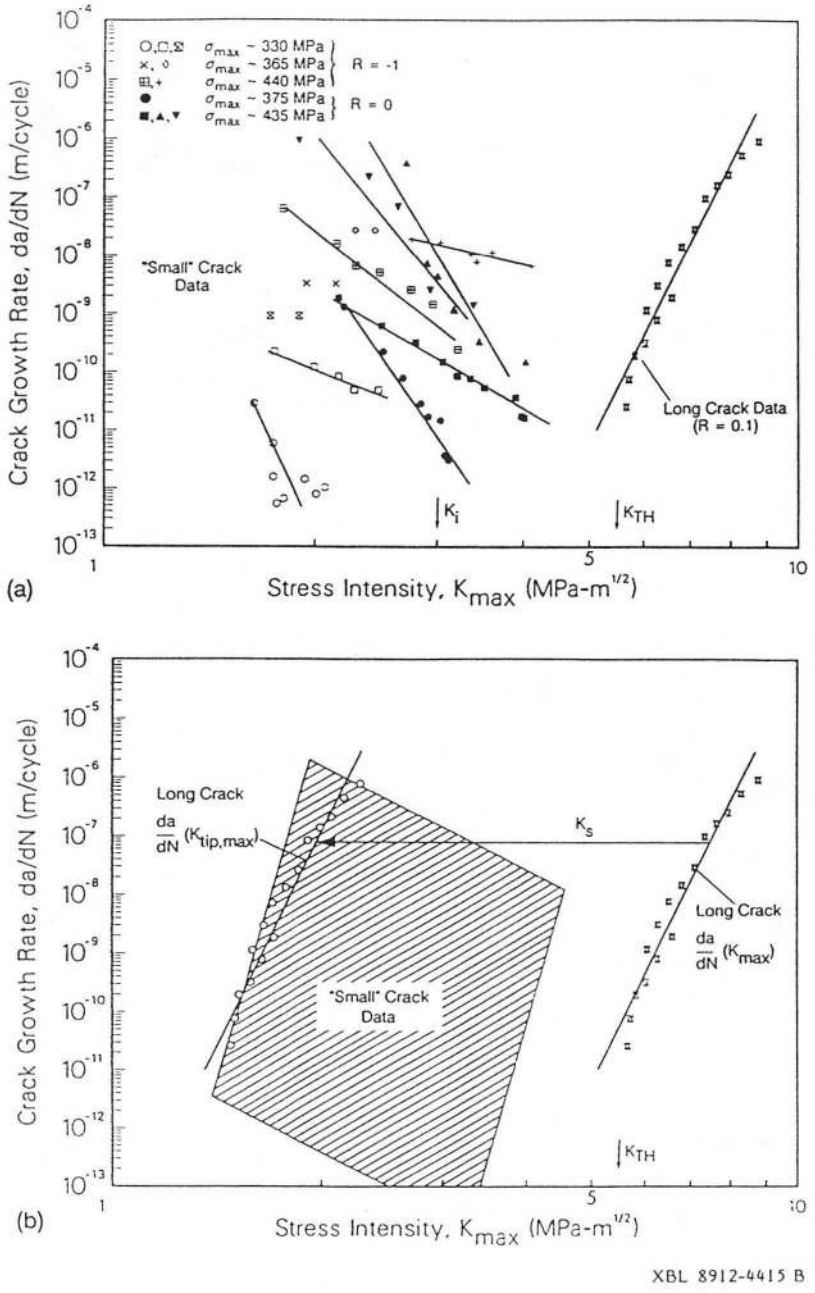

Figure 14: Small-crack growth-rate data in MS-grade Mg-PSZ from cantilever-bend specimens, as a function of K_{max} at R = 0 and -1, compared to corresponding long-crack data as a function of the maximum applied stress intensity in a), and b) showing schematically small-crack data compared to the near-tip stress-intensity relationship for the long-crack data computed from Eq. 6. Note how small cracks propagate at stress-intensity levels well below the long-crack threshold, ΔK_{TH}, for cyclic crack-growth, and even below the initiation toughness, K_i, for monotonic loading in a); initial growth, however, occurs at stress intensities typical of unshielded long cracks in b).[8)]

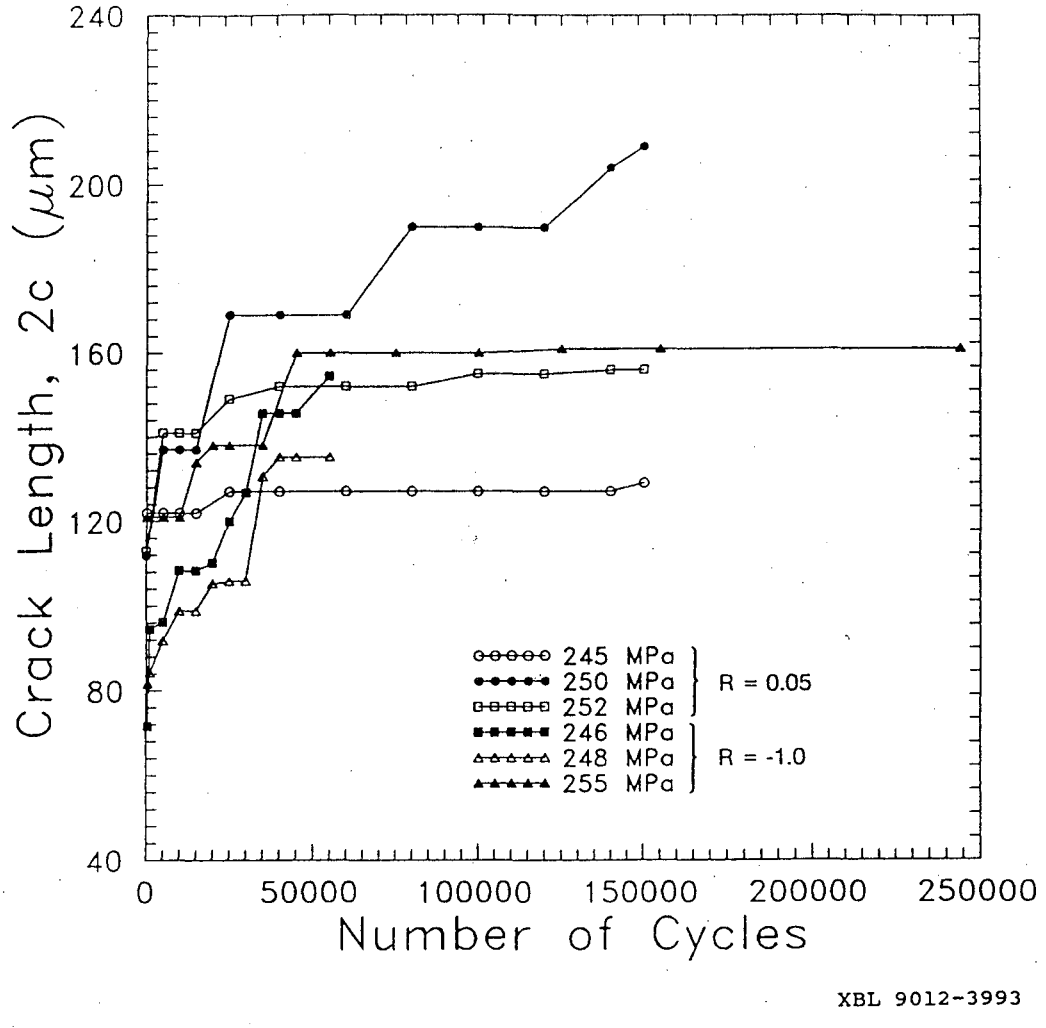

Figure 15: Small-crack data from micro-indented cantilever-bend samples of a Al_2O_3-SiC_w composite, showing comparison of surface crack length 2c vs. number of cycles results for tension-tension (R = 0.05) and tension-compression (R = -1.0) cycling at similar applied stress levels.[33]

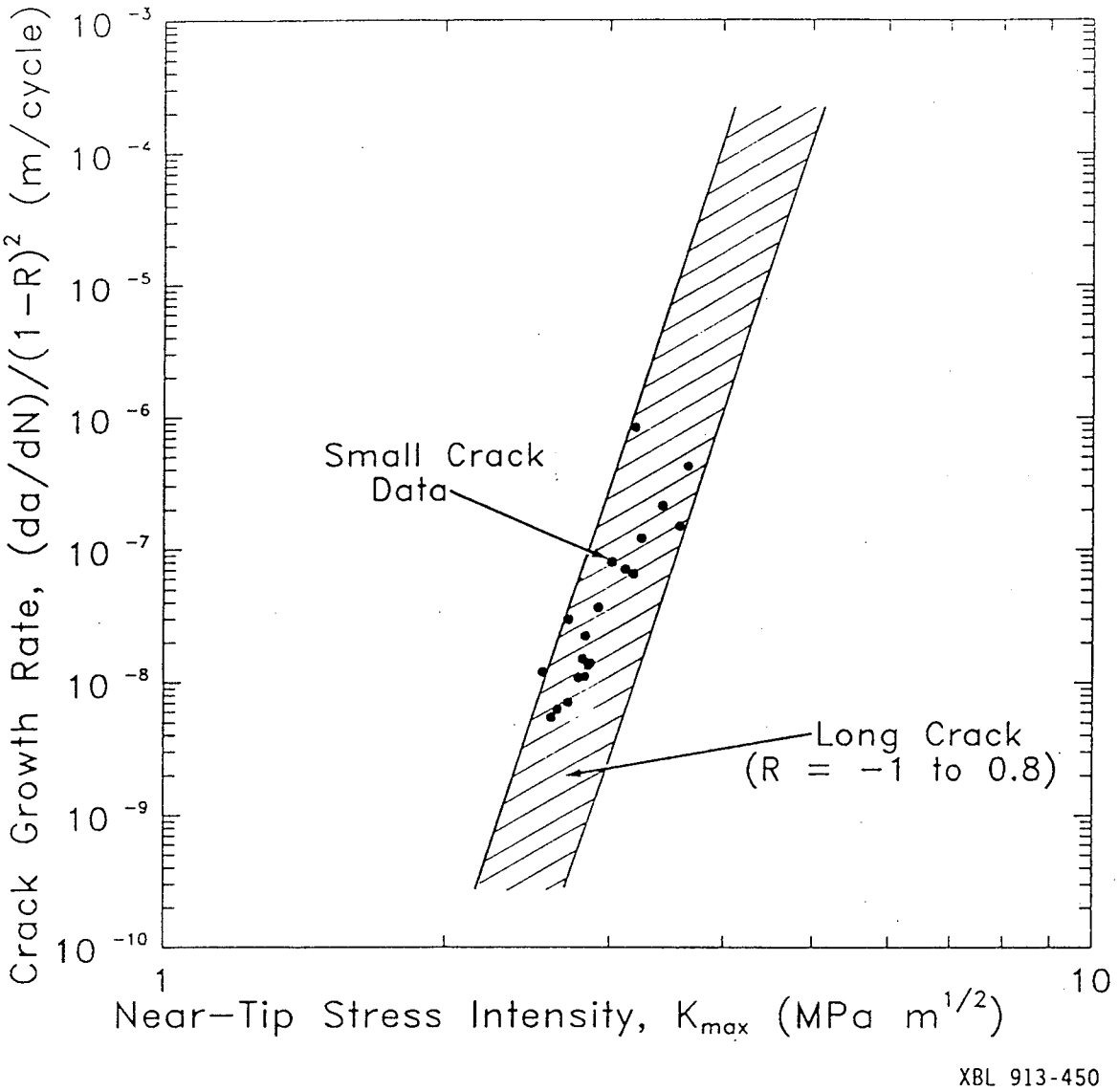

Figure 16: Small-crack growth rates emanating from micro-indents in cantilever-bend samples of 3Y-TZP, plotted as a function of a) the nominal stress intensity, K_{max}, and b) the near-tip stress-intensity, $K_{tip,max}$ (= K_{max} - K_s), after correcting for shielding due to the residual stress field of the indent. Note in b) how, when characterized in terms of the near-tip stress intensity, a close correlation is obtained between long and small crack results.[10]

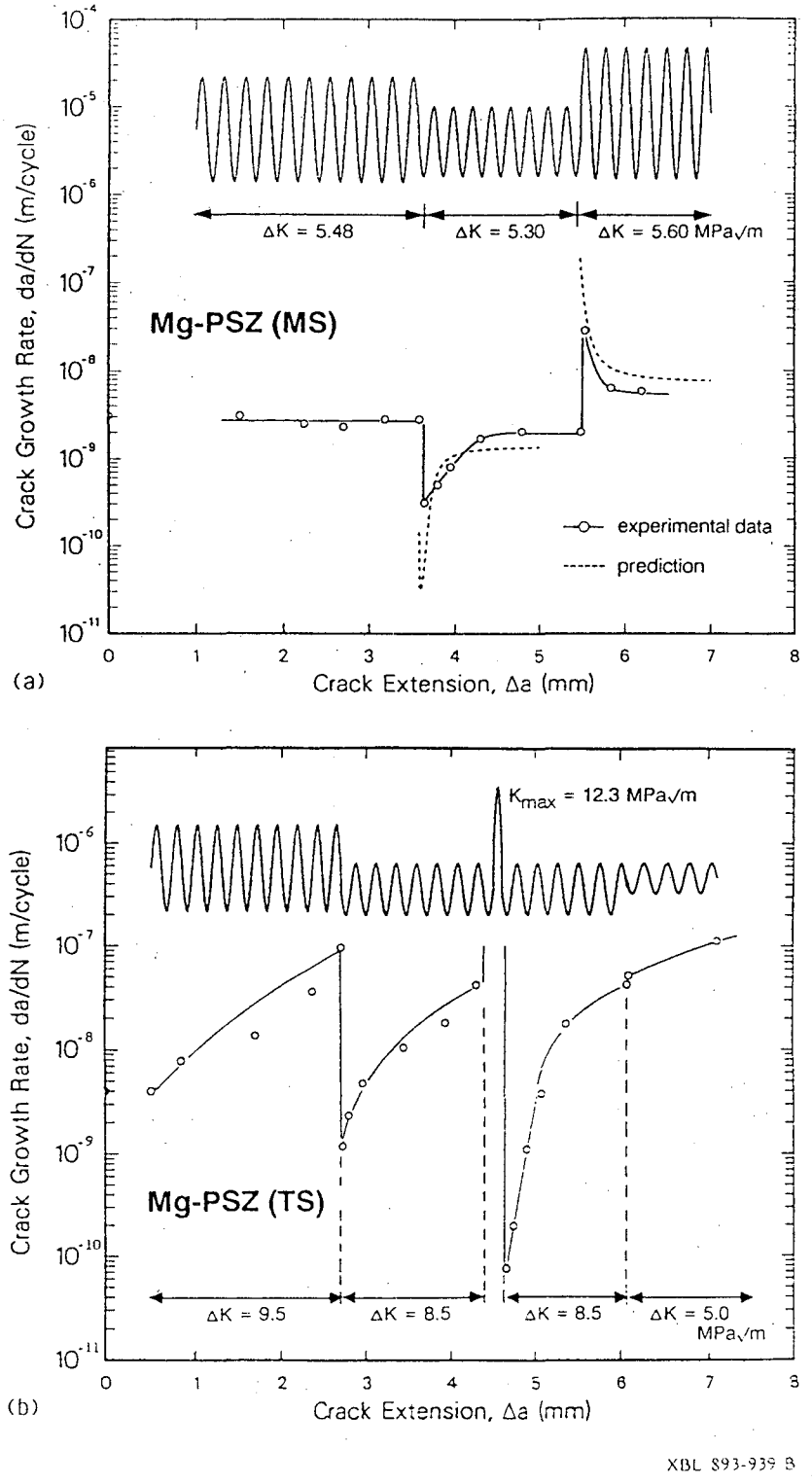

Figure 17: Transient fatigue-crack growth behavior in a) MS-grade Mg-PSZ, and b) TS-grade Mg-PSZ, showing variation in crack-growth rates following high-low and low-high block overloads and single-tensile overloads. Predictions of transient crack-growth behavior in a) rely on steady-state crack-growth data (Fig. 8) and transformation-zone size measurements using Raman spectroscopy (Fig. 18)[49] to compute the crack-tip "driving force" following load changes.[5]

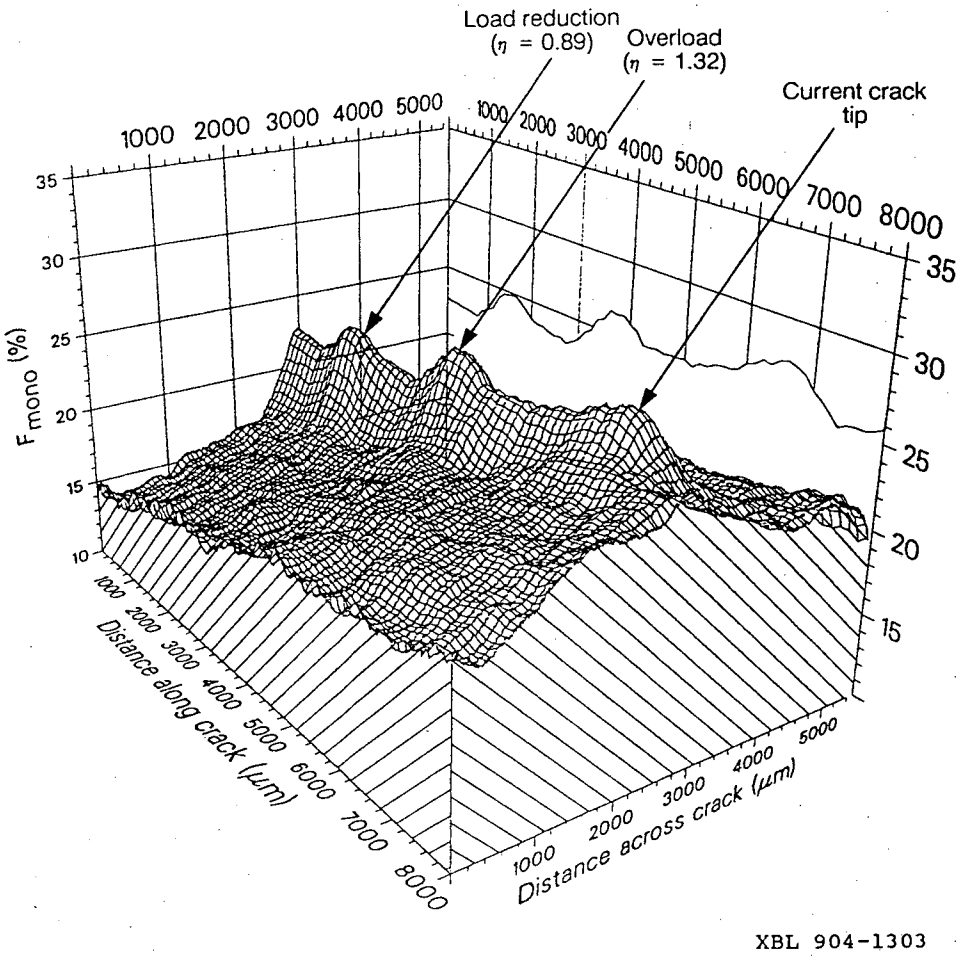

Figure 18: Morphology of the transformation zone, indicated by the volume fraction of transformed phase, F_{mono}, surrounding a fatigue crack in TS-grade Mg-PSZ, following the variable-amplitude loading sequence shown in Fig. 17. The extent of transformation is clearly observed to respond to the applied loading conditions.[5] Results are derived from Raman spectroscopy measurements.[5),49]

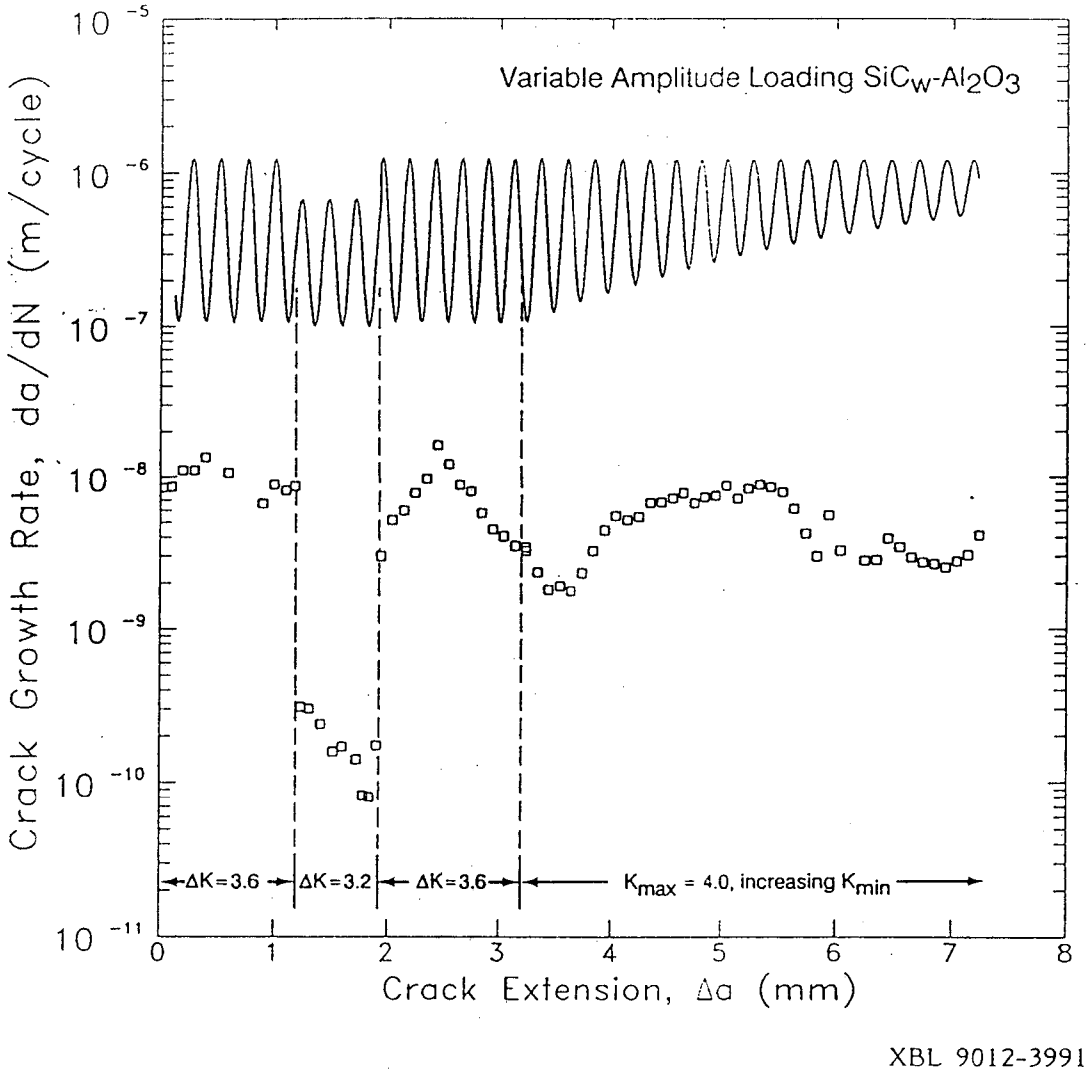

Figure 19: Transient fatigue-crack growth behavior in a SiC-whisker-reinforced alumina composite, showing variation in growth-rates following high-low, low-high and constant-K_{max}/variable-R (increasing K_{min}) block-loading sequences.[33]

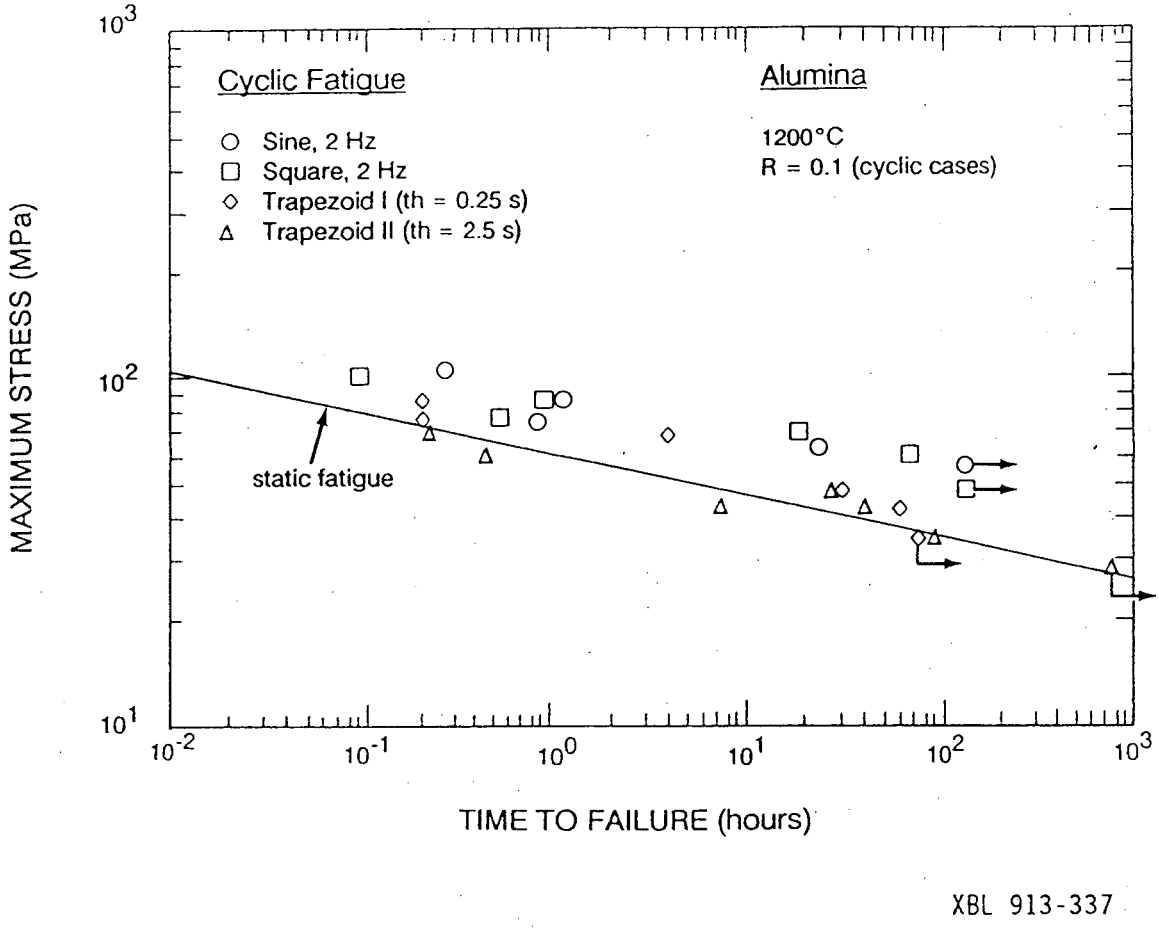

Figure 20: Elevated temperature (1200°C) stress/life data for a commercial polycrystalline alumina, tested in uniaxial tension (R = -1 for cyclic tests), showing a comparison of results for cyclic and quasi-static loading. Note that in contrast to behavior at ambient temperatures (Fig. 2a), at a given applied stress, the cyclic fatigue samples do not necessarily yield the shortest lives.[22]

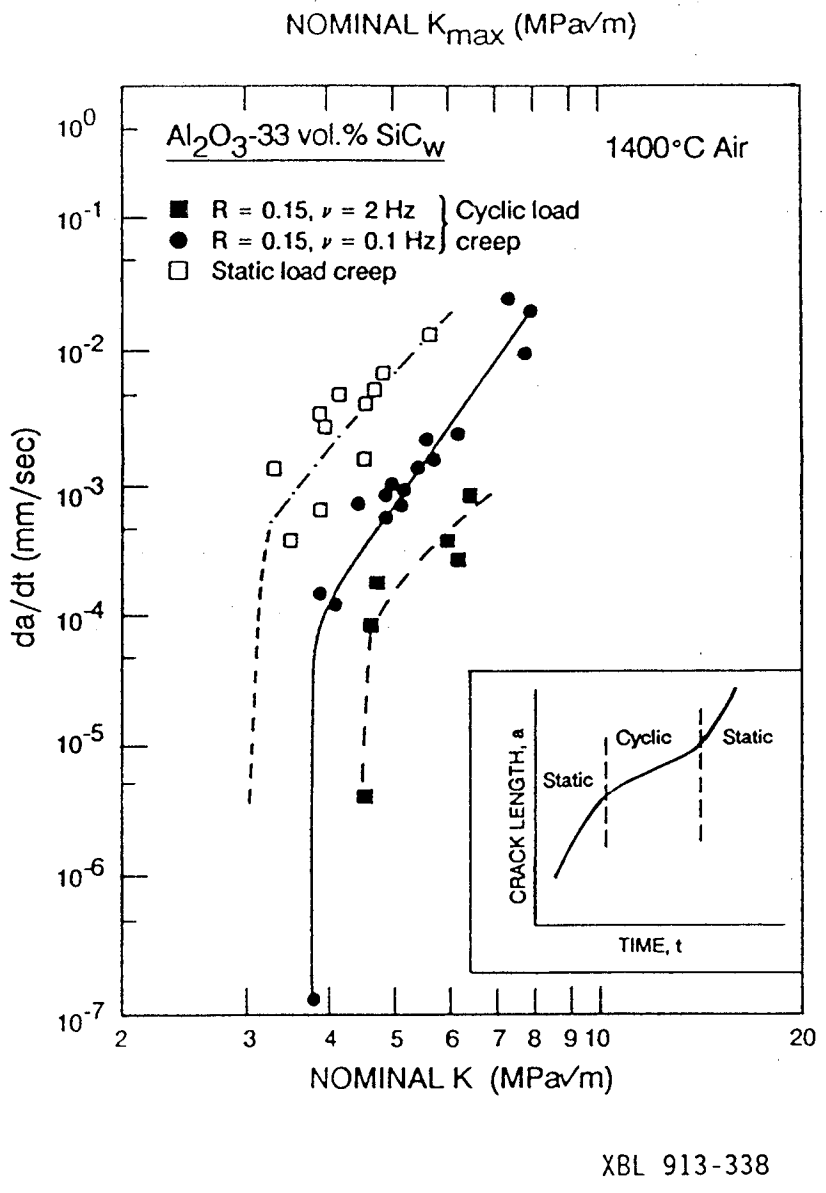

XBL 913-338

Figure 21: Elevated temperature (1400°C) crack-propagation data for a SiC-whisker-reinforced alumina, tested in four-point bending (R = 0.15 for cyclic tests), showing a comparison of results for cyclic and quasi-static loading. Note that in contrast to behavior at ambient temperatures (Fig. 11), at a given applied stress intensity, the cyclic fatigue samples do not yield the fastest crack velocities.[32]

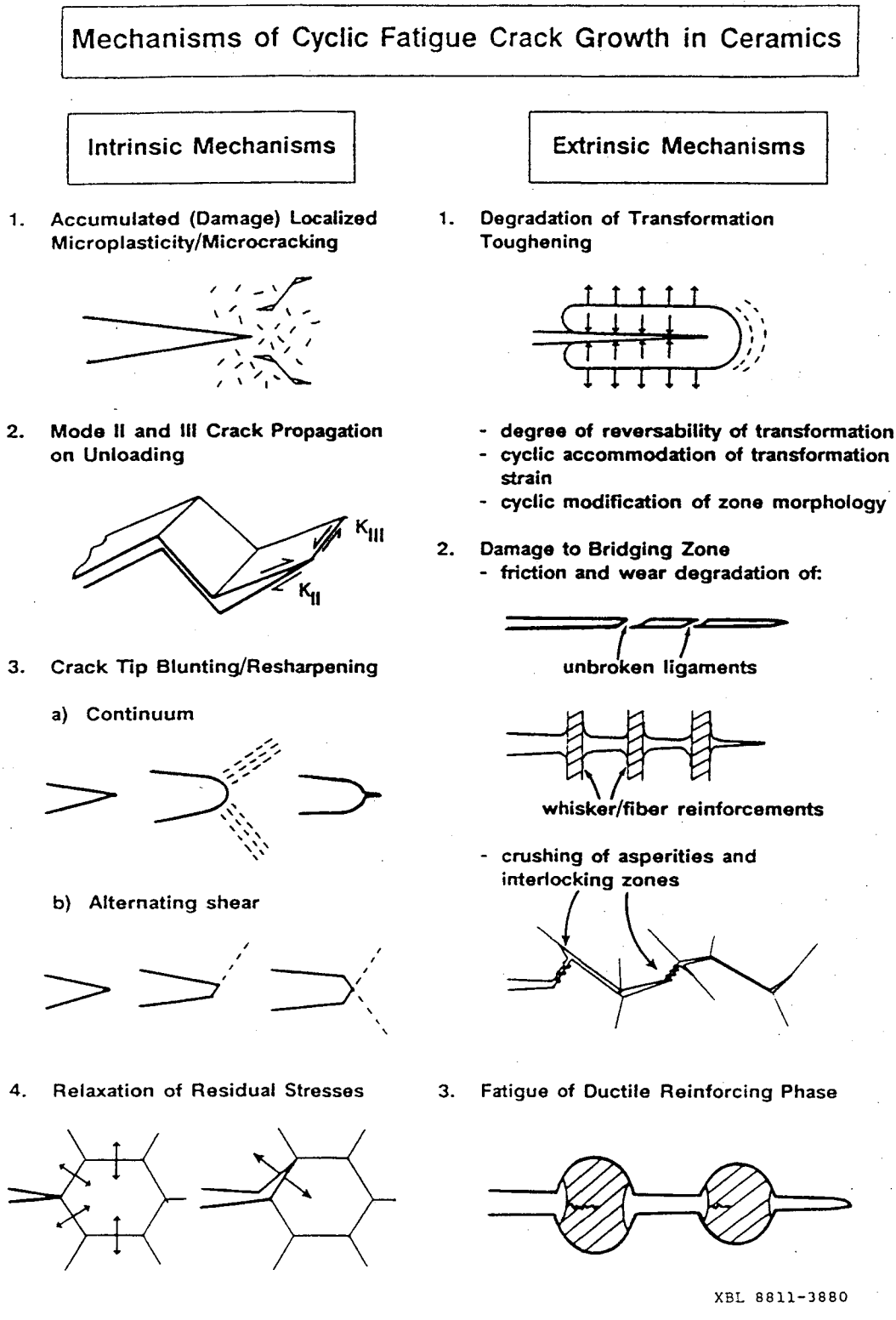

Figure 22: Schematic illustration of possible crack-advance micro-mechanisms during cyclic fatigue-crack propagation in monolithic and composite ceramics.[12]

LAWRENCE BERKELEY LABORATORY
CENTER FOR ADVANCED MATERIALS
1 CYCLOTRON ROAD
BERKELEY, CALIFORNIA 94720